Experimental and Theoretical Study on the Effect of Wall Roughness on the phenomenon "End of the Vortex" in Swirl Tubes

Master Thesis in Process Technology by Torill Rødland Skorve

Department of Physics and Technology
University of Bergen
Norway

November 2011

Acknowledgements

In the present work of my master thesis, many people have been a great help and given inspiration throughout the whole process.

First I want to thank my supervisor Professor Alex C. Hoffmann for his help, guidance and good conversations throughout the work of this thesis. I would give a huge thanks to PhD candidate Gleb Pisarev for his help and collaboration through our common work with the experimental and computational work. His help has been indispensable. Thanks to the Mechanical workshop at University of Bergen who built the experimental rig used in the experimental work. I would also thank Darren White for his help in reading the text and correcting the language in this thesis.

I would also use this opportunity to thank my fellow students at UoB.

Finally, I would like to thank my husband Helge Skorve who has always been a great support throughout my time as a student. My thanks also goes to my parents Arne and Anne M. Rødland for great support, and for help with taking good care of my daughter.

Abstract

In this thesis, a combination of experimental measurements and numerical simulations are used to investigate the phenomenon "End of the Vortex" in swirl tubes. The main focus here has been comparing swirl tubes containing walls with smooth surfaces to tubes with different heights of wall roughness. The tubes containing wall roughening were either treated with sandpaper or metal particles to achieve a uniform roughening at the wall throughout the whole section. The vortex has been visualized by two different methods; by inserting dust into the tube and by the use of high resolution pressure transducers on the separator tube.

The experiments were carried out on different cylindrical tubes with lengths of 60, 80 and 100 cm. The effect of flow rate through the cyclone was studied. The results of the experimental measurements are compared with data from numerical simulations. 3-D RSM simulations were carried out using the commercial CFD package Star-CD. The obtained results showed qualitative agreement with each other. The results showed that the vortex core bent off to the wall further up in the separator tube when the walls contained a rough surface. The vortex also needed a higher flow rate before it went down to the bottom and centralized than it needed with a smooth surface.

Contents

Acknowledgements i

Abstract iii

List of Figures ix

List of Tables xi

List of Symbols xiii

1 Introduction 1

1.1 Relevance . . . 1

1.2 Technological Background . . . 1

1.2.1 Cylinder-on-cone . . . 2

1.2.2 Swirl Tube . . . 4

1.3 A Short Introduction to the Phenomenon End of the Vortex . . . 4

1.4 Goal of this Thesis . . . 5

2 Theory 7

2.1 Forces in Vortex Flow . . . 7

2.1.1 Centrifugal Force . . . 9

2.2 Flow Pattern and Velocity Profiles in Cyclones . . . 9

2.2.1 The Main Flow Pattern . . . 10

2.2.2 Axial Velocity . . . 10

2.2.3 Tangential Velocity . . . 11

2.2.4 Radial Velocity . . . 12

2.3 Cyclone Pressure Drop . . . 13

2.3.1 Euler Number . . . 15

2.4 Separation Efficiency . . . 15

2.4.1 Overall Separation Efficiency . . . 15

2.4.2 Grade-Efficiency . . . 16
2.4.3 Cut Size . . . 17
2.5 End of the Vortex . . . 17
2.5.1 Factors that Affects the End of the Vortex . . . 18
2.6 The Natural Vortex Length . . . 25
2.6.1 Models Predicting the length of the Natural Vortex . . . 25
2.7 Computational Fluid Dynamics . . . 26
2.7.1 Background and History . . . 26
2.7.2 Turbulence Models . . . 27
2.7.3 Modelling of Wall Friction . . . 29

3 Literature survey **31**
3.1 End of the Vortex . . . 31
3.1.1 Alexander [1949] [1] . . . 31
3.1.2 Hoffmann et al. [1995] [17] . . . 31
3.1.3 Peng et al. [2005] [30] . . . 32
3.1.4 Cuizhi et al. [2010] [12] . . . 32
3.1.5 Pisarev et al. [2010] [31] . . . 32
3.1.6 Pisarev et al. [2011] [32] . . . 33
3.2 Wall Roughness . . . 33
3.2.1 Kaya et al. [2011] [21] . . . 33

4 Experimental Setup and Numerical Boundaries Conditions **35**
4.1 Description of the Swirl Tube and its Equipment used in the Experiments 35
4.1.1 The Separator Body . . . 36
4.1.2 Swirl Vanes . . . 37
4.1.3 Vortex Finder . . . 38
4.1.4 Pressure Transducers and Tappings . . . 39
4.1.5 Wall Roughness . . . 40
4.2 Performance of the Experiments on the Swirl Tube . . . 41
4.2.1 Measurement of the Flow Rate . . . 41
4.2.2 Observation of the Flow with Dust Injected . . . 42
4.2.3 Measurement with Pressure Transducers . . . 43
4.3 Computational Setup . . . 44
4.3.1 Software and Simulation Preference . . . 44

5 Results and Discussion **47**
5.1 Comparison With Earlier Work on the Project 47
5.1.1 60 cm Swirl Tube 48
5.1.2 80 cm Swirl Tube 49
5.1.3 100 cm Swirl Tube 51
5.1.4 Standard Deviation of the Flow Rate from the Centrifugal Pump 53
5.2 Measurement with Pressure Transducers 55
5.3 Measurements on a Swirl Tube with Varying Wall Roughness 63
5.3.1 Walls Treated with Sandpaper. 63
5.3.2 Walls Coated with Metal Particles. 64
5.3.3 Computational Results 65
5.3.4 Comparison of Experimental and Numerical Results 68
5.4 Sources of Error 69

6 Conclusions **71**

7 Further Research **73**

A Venturi Flowmeter **75**

B Tables **79**

C Standard Deviation of the Pump **83**

D Measurements with Pressure Transducers **85**
D.1 80 cm swirl tube 85
D.1.1 The flow rate at 67 m^3/h 85
D.1.2 The flow rate at 156.6 m^3/h 86
D.2 100 cm swirl tube 88
D.2.1 The flow rate at 111.1 m^3/h 88

List of Figures

1.1 Sketch of the tangential and axial inlet.
1.2 Illustration of cylinder-on-cone and swirl tube cyclones.
1.3 Sketch of a centralized vortex and precessing vortex in a swirl tube.
2.1 Sketch of the Rankine vortex curve.
2.2 Sketch of the centrifugal force.
2.3 Sketch of the centripetal force.
2.4 Illustration of the flow pattern.
2.5 Sketch of the axial velocity profile.
2.6 Sketch of the tangential velocity profile.
2.7 Sketch of a grade-efficiency curve.
2.8 Illustration of the precessing vortex core.
4.1 Sketch of the experimental setup of the test rig.
4.2 A picture and a sketch of the separator body.
4.3 Illustration and a picture of the swirl vanes.
4.4 Illustration and a picture of the vortex finder.
4.5 A picture of a pressure transducer.
4.6 A picture of the pressure tappings on the separator body.
4.7 A picture of the separator tube covered with metal particles.
4.8 A sketch of the vortex core passing the pressure tappings while it is bending to the wall and precessing around it.
4.9 An overview of the CFD model.
5.1 A graph showing the results from an 35+20 and 60 cm separator tube.
5.2 A graph giving the results from an 35+40 cm, 80 cm and 35+50 cm tube.
5.3 A graph showing the comparison of the results from an 35+40+20 cm and 100 cm tube.
5.4 A graph showing the values of centralization from the different tubes compared to the old experiments.
5.5 A picture showing the pressure profile of the "end of the vortex" in a swirl tube.
5.6 Output from LabView. Pressure measured at a point 29 cm from the swirl vanes in a 60 cm tube at flow rate of 173 m^3/h.
5.7 Output from LabView. Pressure measured at a point 32 cm from the swirl vanes in a 60 cm tube at flow rate of 173 m^3/h.
5.8 Output from LabView. Pressure measured at a point 29 cm from the swirl vanes in a 60 cm tube at flow rate of 102 m^3/h.

5.9 Output from LabView. Pressure measured at a point 32 cm from the swirl vanes in a 60 cm tube at flow rate of 102 m^3/h.
5.10 Output from LabView. Pressure measured at a point 29 cm from the swirl vanes in a 60 cm tube at flow rate of 72.8 m^3/h.
5.11 Output from LabView. Pressure measured at a point 29 cm from the swirl vanes in a 60 cm tube at flow rate of 72.8 m^3/h.
5.12 A presentation of the EoV where the vortex centralizes in 3 tubes of 60 cm, containing different inner wall roughness.
5.13 A presentation of the EoV where the vortex centralizes in 3 tubes of 80 cm, containing different inner wall roughness.
5.14 CFD simulation with flow rate of 200 m^3/h. Picture of a centralized vortex and a precessing vortex.
5.15 CFD simulation with flow rate of 200 m^3/h.
A.1 An illustration of a venturi flowmeter.
D.1 Output from LabView. Pressure measured at a point 28 cm from the swirl vanes in a 80 cm tube at a flow rate of 67 m^3/h.
D.2 Output from LabView. Pressure measured at a point 34 cm from the swirl vanes in a 80 cm tube at a flow rate of 67 m^3/h.
D.3 Output from LabView. Pressure measured at a point 28 cm from the swirl vanes in a 80 cm tube at a flow rate of 156.6 m^3/h.
D.4 Output from LabView. Pressure measured at a point 34 cm from the swirl vanes in a 80 cm tube at a flow rate of 156.6 m^3/h.
D.5 Output from LabView. Pressure measured at a point 28 cm from the swirl vanes in a 100 cm tube at a flow rate of 111.1 m^3/h.
D.6 Output from LabView. Pressure measured at a point 31 cm from the swirl vanes in a 100 cm tube at a flow rate of 111.1 m^3/h.

List of Tables

5.1 Measurement of the flow rate in a 60 cm tube with smooth walls.
5.2 Measurement of the flow rate in a 80 cm tube with smooth walls.
5.3 Measurement of the flow rate in a 100 cm tube with smooth walls.
5.4 Pressure drop over the 60 cm tube at flow rate of 173 m^3/h.
5.5 Pressure drop over the 60 cm tube at flow rate of 102 m^3/h.
5.6 Pressure drop over the 60 cm tube at flow rate of 72.8 m^3/h.
5.7 Pressure drop over the 80 cm tube at flow rate of 67 m^3/h.
5.8 Pressure drop over the 80 cm tube at flow rate of 156.6 m^3/h.
5.9 Pressure drop over the 100 cm tube at flow rate of 111.5 m^3/h.
5.10 Difference in wall roughness versus time, from measurement of 60 cm and 80 cm separator tube treated with sandpaper.
5.11 Measurement of the flow rate in a 60 cm tube coated with metal particles.
5.12 CFD results.
B.1 Measurement of the flow rate in a 60 cm tube with smooth walls.
B.2 Measurement of the flow rate in a 60 cm tube with smooth walls.
B.3 Measurement of the flow rate in a 80 cm tube with smooth walls.
B.4 Measurement of the flow rate in a 80 cm tube with smooth walls.
B.5 Measurement of the flow rate in a 100 cm tube with smooth walls.
C.1 Measurement of the flow rate in a 60 cm tube at low flow rates. Values used to calculate the standard deviation.

List of Symbols

A	area		m^2
A_i	inlet area		m^2
a	height of cyclone inlet		m
B	empirical constant for smooth walls		
b	width of cyclone inlet		m
C	constant		
C_{ij}	convection term		
C_d	discharge coefficient 0.90		
D	diameter of cyclone body		m
De	diameter of cyclone vortex finder		m
D_{ij}	diffusion term		
E	log-law coefficient		
E'	wall function coefficient		
Eu	Euler number	$\frac{\Delta p}{\frac{1}{2}\rho\nu^2}$	
ε	dissipation term		m^2/s^3
f	friction factor		
G_θ	axial flux of angular momentum		kg m^2/s
G_x	axial flux of axial momentum		kg m^2/s
g	gravity constant		m/s^2
h	hight		m
κ	Von Karman constant 0.42		
Ln	natural vortex length		m
M	mass of solids		kg
m	mass		kg
η	overall fractional separation efficiency		
μ	viscosity		Pa s
ν	kinematic viscosity		m^2/s
P_{ij}	generation or production term		
p	pressure		Pa
Φ_{ij}	pressure-strain term		Pa
ϕ	angle (degree)		
Q	flow rate		m^3/h
ρ	gas density		kg/m^3

Re	Reynolds number	$\frac{\rho u D}{\mu}$	
R^+	roughness parameter		m
R_x	radius of vortex finder		m
r	radius		m
r	radial coordinate		m
r_h	roughness height		m
r_o	outer radius		m
S	swirl number	$\frac{G_\theta}{G_x R_x}$	
τ_w	wall shear stress		$\mathrm{N/m^2}$
U_0	voltage at zero pressure		V
$U_{measured}$	measured voltage		V
u_τ	friction velocity		m/s
u^+	wall-parallel velocity		m/s
V_{in}	inlet velocity		m/s
v	velocity		m/s
v_θ	tangential kinematic viscosity		$\mathrm{m^2/s}$
$v_{\theta,w}$	tangential velocity at the wall		m/s
v_{in}	inlet velocity		m/s
v_z	axial velocity		m/s
z	axial coordinate		m
Ω	angular velocity		$\mathrm{s^{-1}}$

Chapter 1

Introduction

1.1 Relevance

Centrifugal separators have long been used in industry to separate out both solids and liquids to provide a clean gas. Cyclones are widely used in the oil and gas industry where they are used in for example Fluidized Catalytic Cracking of hydrocarbons (FCC) and natural gas. They are also used for demisting (pharmaceutical industry), nutrition, paper and pulp and in the energy industry. In the future it is believed that they could be used in in-line technology as well [19], [27]. The most important reasons for the use of cyclones are that they are inexpensive to purchase, they have no moving parts, and they can be constructed to withstand harsh operating conditions [24].

1.2 Technological Background

This thesis is written as a part of an ongoing research project in collaboration with the Department of Physics in the University of Utrecht. The project is founded by the Norwegian Research Council under the FRINAT program.

Centrifugal separators, also called cyclone separator have been used in industry for more than 100 years, and are one of the most widely used of all industrial gas cleaning devices [19]. The first patent was granted in the United States by John M. Finch in 1985 for the Knickerbocker Company [18].

A centrifugal separator is a simple device that forces the incoming particle laden flow into a spiral motion and separates the particles from the main flow under the action of centrifugal forces [21].

There are many advantages to using cyclones as a gas cleaning equipment, as opposed to other methods of separation. Some important factors are that they can operate under

difficult conditions such as high temperatures and pressures or with chemically aggressive feeds. Low maintenance requirements because there are no moving parts and low capital cost [31], [32].

The main disadvantage of using cyclones is that they have a low collection efficiency for particles with a size lower than the cut-size, which is normally 1 to 5 microns. Other disadvantages worth mentioning are that they need a higher pressure drop than other separating equipment, and they are prone to clogging and erosion, depending on the nature of the particles and the flow pattern in cyclones [15], [19].

Cyclone design in general consist of two types of design: the stright-through cyclone and the reverse-flow cyclone. The last one is the most common type in industry [6]. The reverse-flow separators, of all shapes and sizes, are used for dedusting and demisting gases. There are several types of centrifugal separators, but those that are in most common use in industry are:

- Cylinder-on-cone
- Swirl tube

These two types are both of the reverse-flow type, see later in this section [19]. The main focus in this thesis are centrifugal gas cleaning devices, where cyclones are used as gas-solids separators for dedusting.

1.2.1 Cylinder-on-cone

The cylinder-on-cone cyclone with a tangential inlet and two axial outlets for clean gas and collected dust respectively, is the most common design for a cyclone in industry [19]. A sketch of a tangential inlet shown from a top view are given in Figure 1.1 a). This type of inlet are being most used in the petroleum processing industries [18].

The design of the cyclone body normally consists of a cylindrical tube on top, connected to a conical one at the bottom. See Figure 1.2 a).

In a standard reverse-flow cylinder-on-cone cyclone, a double swirling flow is created in the separation space by the tangential entrance of the gas. On the outer part, the gas flows downward. When the swirl reaches the bottom, it reverses itself and moves upward in the center [12].

A disadvantage for cylinder-on-cone cyclones are that they are prone to clogging depending on the flow pattern in the cyclone [19].

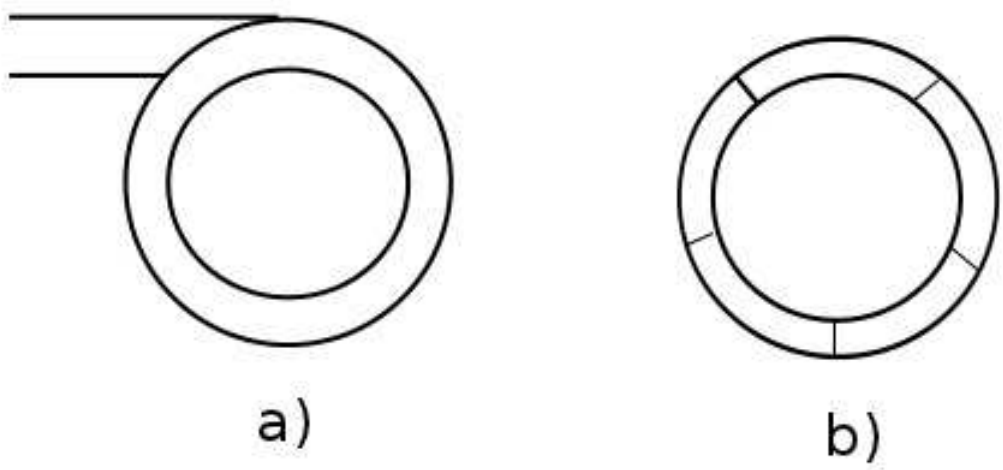

Figure 1.1: Sketch of a) tangential inlet from the top, and b) an axial inlet with swirl vanes from the top.

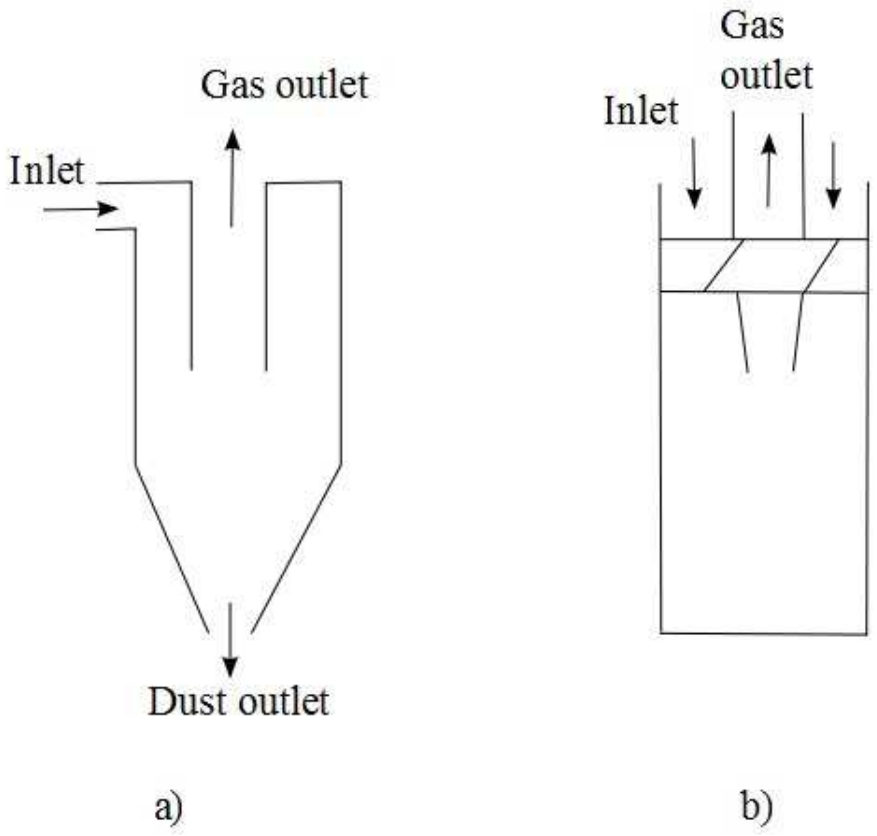

Figure 1.2: Sketch of a) cylinder-on-cone with tangential inlet, and b) swirl tube with axial inlet.

1.2.2 Swirl Tube

Swirl tubes are a special type of cyclone [19]. In fluidized catalytic cracking they are often used in the final-stage gas cleaning with moderate or low solids loading and is often operating with many tubes in parallel arranged in so-called "swirl decks" [26], [28]. A sketch of swirl tube with axial inlet is shown in Figure 1.2 b).

A swirl tube is a centrifugal separator which is often shaped like a cylindrical tube. It has an axial inlet and contains swirl vanes, which are curved blades. A sketch of the swirl vanes with an axial inlet are given in Figure 1.1 b). The in and outflow in swirl tubes moves along the same axis [19]. In a reverse-flow centrifugal separator the gas enters at the top, and the swirl vanes causes the airstream downward on the outer part of the tube. Centrifugal force and inertia cause the particles to move outward and collide with the outer wall before it slide down to the bottom of the tube. Near the bottom of the cyclone, the gas reverses its axial flow direction and moves upward in a smaller inner spiral and exits from the top through a vortex finder. The particles would usually be taken out at the bottom of the tube through a dust hopper [9].

Swirl tubes are easier to construct than cylinder-on-cone cyclones, and they also have high mechanical integrity. They are less prone to clogging then cylinder-on-cone separators. The swirl vanes delivers a strongly swirling flow that centrifuges the particle to the wall on their way to the solids outlet [28]. Another advantage for swirl tubes are the use of axial inlet by their use of swirl vanes. This type of entry has a high degree of axial symmetry in the flow, which gives operational advantages since it eliminates the region on the inside of the vortex finder, which are prone to clogging [18].

The main uses of swirl tubes is cleaning industrial gases, separation of catalyst from reactive gases and cleaning of exhaust gases before power recovery systems, dedusting from hot gases, dehydration, separation of oil and water, on offshore installation or underground where space is limited [28], [34].

Throughout this thesis, the word cyclone is used for both cylinder-on-cone cyclones with tangential inlet and for swirl tubes containing swirl vanes and axial inlet.

1.3 A Short Introduction to the Phenomenon End of the Vortex

A good understanding of the phenomenon "End of the Vortex" (EoV) is necessary for improving cyclones like swirl tubes and cylinder-on-cones performances. This flow phenomenon is an instability that may occur spontaneously, low in the cyclone [30]. When that happens, the vortex core will bend off from its axial position and attach itself to the wall. The presence and position of EoV is essential for the separator performance because it affects the efficiency. The presence may also cause clogging and wear in operating cyclones. A sketch of this phenomenon is shown in Figure 1.3 b). When this

phenomenon is not present, the vortex core will coincide with the axis of the cyclone, and the vortex will extend all the way to the bottom. This is sketched in Figure 1.3 a).

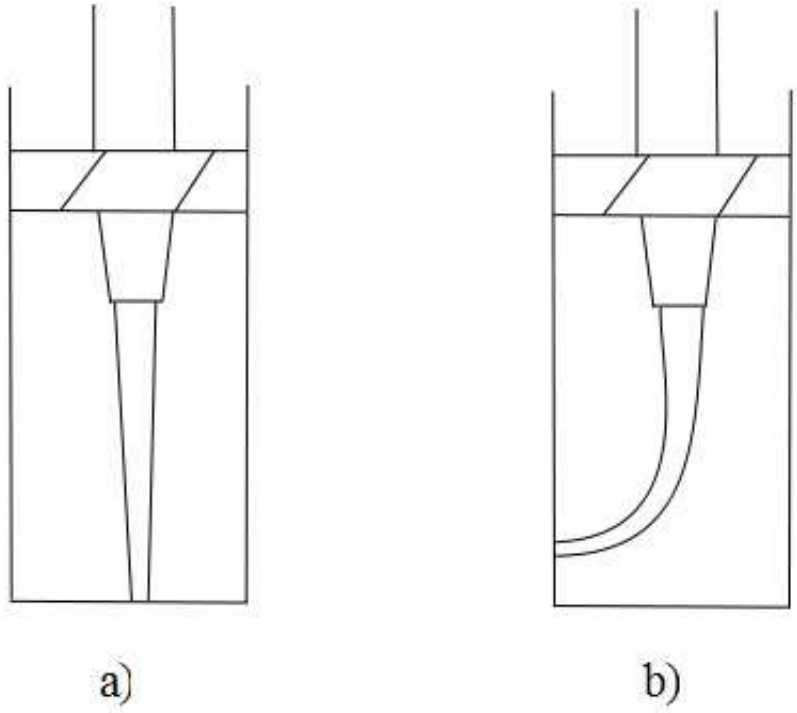

Figure 1.3: a) Centralized vortex core. b) End of the vortex.

This thesis will be about the phenomenon EoV, and how the effect of wall roughness influences its behaviour in general. The results are in print for being published, and can be useful information for improvement of cyclone design.

1.4 Goal of this Thesis

The background for this thesis are to study the flow phenomenon end of the vortex in a swirl tube. Even though there have been performed many studies of cyclones earlier by different researchers, this phenomenon is not yet fully understood [31]. The work done in the masters thesis of Gjerde [16] will also be continued.

The thesis will consist of theoretical, numerical and experimental studies where Computational Fluid Dynamics (CFD) simulations are used in the numerical part. An experimental test rig of a swirl tube which is located in the basement of the Department of Physics and Technology, UiB is used for the experimental part.

In this rig, tests and observations will be performed on a gas stream in a reverse-flow swirl tube. The results will be compared to previous work done in the same rig, and also be compared to the numerical results from CFD simulations.

The experimental tests will be run on different lengths of cylindrical tubes. Also the wall roughness will be varied in the tests.

The effect of wall roughness on the behaviour of the vortex core and the location of the EoV will also be investigated numerically and the result of this will be compared to the experimental results.

Chapter 2

Theory

2.1 Forces in Vortex Flow

The swirling motion from a vortex flow occurs in different equipment like cyclones, hydrocyclones, spray dryers and vortex burners. The tangential velocity distribution can exhibit two types of ideal swirling flows:

- forced vortex flow
- free vortex flow

The forced vortex flow is a swirling flow that has the same tangential velocity distribution as a rotating solid body. The free vortex flow behaves the same way a frictionless fluid does, and the tangential velocity in the swirl is such that the moment-of-momentum of the fluid elements is the same at all radii. The tangential velocity distribution is between these two swirling flows in real swirling flows [19].

If the swirling fluid has an infinite viscosity, which means that it behaves like a solid body, no shearing motion will exist between the fluid layers at different radii. The fluid elements are forced to have the same angular velocity, Ω. Swirl with a constant angular velocity is called forced vortex flow.

$$v_\theta = \Omega r \tag{2.1}$$

This equation is called the first ideal swirl flow, where v_θ is the tangential velocity and r represents the radial coordinate.

If the swirling fluid has no viscosity, the neighbouring elements will not affect the motion of a given fluid element. The tangential velocity will increase if an element with a smaller

radius is brought into the fluid, since its moment-of-momentum will be conserved. Such a vortex where the moment-of-momentum is conserved, is called frictionless. In these type of flows, C is a constant and gives:

$$v_\theta = \frac{C}{r} \tag{2.2}$$

The Equation (2.2) is called the second ideal swirl flow.

A real fluid will be something in between these two cases. Equation (2.1) and (2.2) can be combined into one equation which is similar to a real vortex flow:

$$v_\theta = \frac{C}{r^n} \tag{2.3}$$

The flow consists of two regions where the outer region of free vortex flow n=1 is surrounding an inner region of forced vortex flow n=-1. This is shown in Figure 2.1, and is called a Rankine vortex [26].

The flow in the outer region is the interesting part when it comes to cyclone modeling. From Equation (2.3), the value for n is usually lower than unity and it depends on several parameters like the wall roughness, cyclone geometry and particle concentration. It usually varies between 0.5 and 0.8.

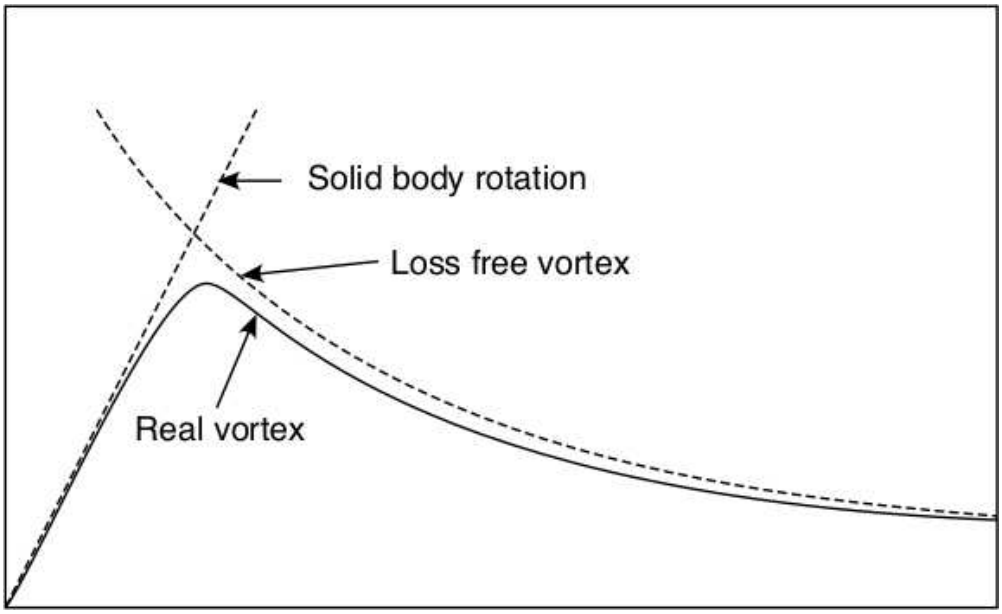

Figure 2.1: The Rankine vortex model is a simple two-equation parametric description of a swirling flow. It is characterized by a free vortex where the inner circular region and forced vortex in the outer region [14].

This flow is similar to a normal vortex flow in centrifugal separators [30].

2.1.1 Centrifugal Force

The centrifugal force is the most important force in a cyclone, since that force is the reason cyclones exist. Separation of particles in cyclones is caused by centrifugal forces, which are a consequence of the swirling motion of the gas. The particles that are denser than the gas are forced to move outward towards the cyclone wall before moving downward to the bottom [18]. It is this outward force that is called the centrifugal force. This force is proportional to the diameter cubed [30]. In Figure 2.2 the centrifugal force for a fluid element is balanced by a force created by a gradient in the static pressure. The force is acting towards the axis of rotation, and makes sure that the element stays in its path [19].

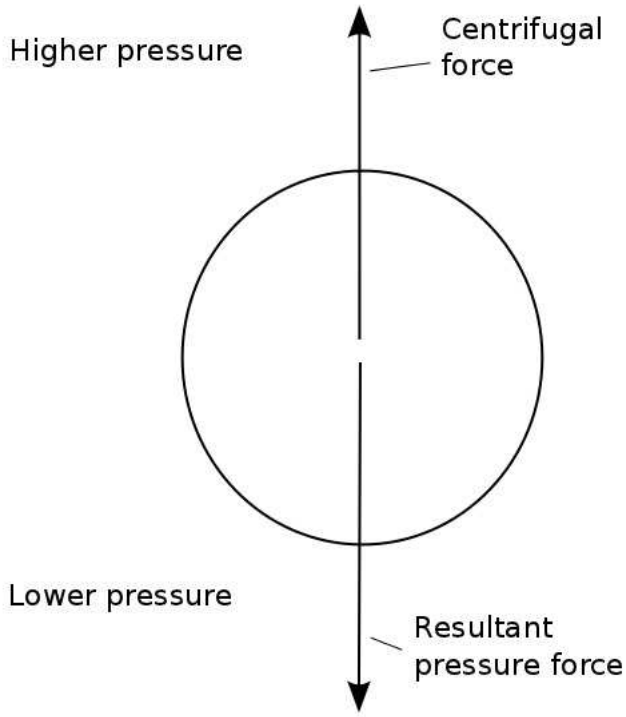

Figure 2.2: Sketch of the centrifugal force.

The centrifugal force which is an apparent force is acting in a coordinate system, and under consideration is turning with particle. In a stationary coordinate system it is actually a centripetal acceleration that the particle undergoes continually to remain in orbit. A sketch of that is shown in Figure 2.4.

2.2 Flow Pattern and Velocity Profiles in Cyclones

Even though the geometry of the cyclone is simple, the pattern of the flow is very complex [8]. The flow pattern in a swirl tube is affected by different parameters such as the length of the swirl tube, geometry of dustbin, cyclone wall roughness, diameter of the vortex

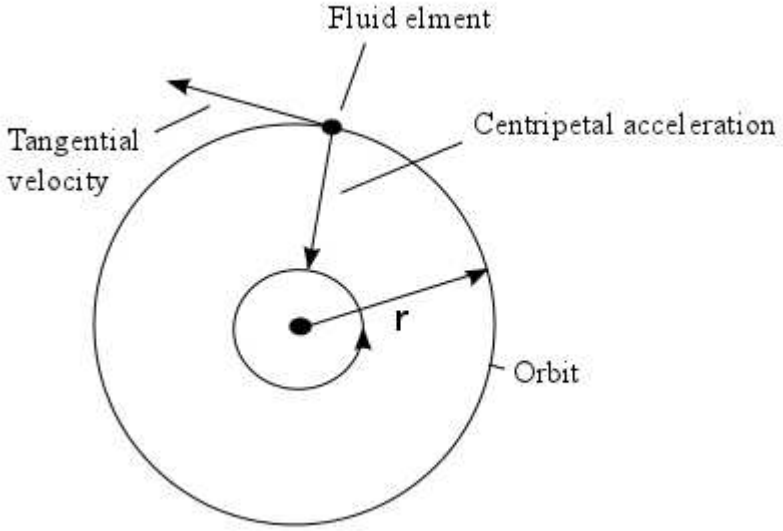

Figure 2.3: Sketch of the centripetal acceleration.

finder, and inlet gas velocity [32]. Sketches of the flow pattern in reverse-flow cyclones can be seen in Figure 2.4.

2.2.1 The Main Flow Pattern

In general, for a reverse-flow cyclone, the flow pattern is dominated by a swirling motion in the separation space. For cylinder-on-cone, this is created by the tangential injection of gas, while for swirl tubes it is generate by swirl vanes. The gas will flow downward close to the wall in the outer part of the swirl. The gas will then flow back up in the center of the cyclone and out through the vortex finder. At the same time a radial flow will occur in the cyclone which moves from the outer vortex to the inner vortex. This flow is distributed over the length of the body underneath the vortex finder [18].

The most important and critical flow in a cyclone is the downward flow at the wall. That flow is the primary mechanism for transporting the captured particle downward to a dust outlet, and not the gravity force [18].

2.2.2 Axial Velocity

As mentioned above in section 2.2.1, the flow with axial velocity is directed downward with an outer position close to the wall, and upward in the inner region near the axis. The downward direction is often referred to as the outer vortex and the upward direction as

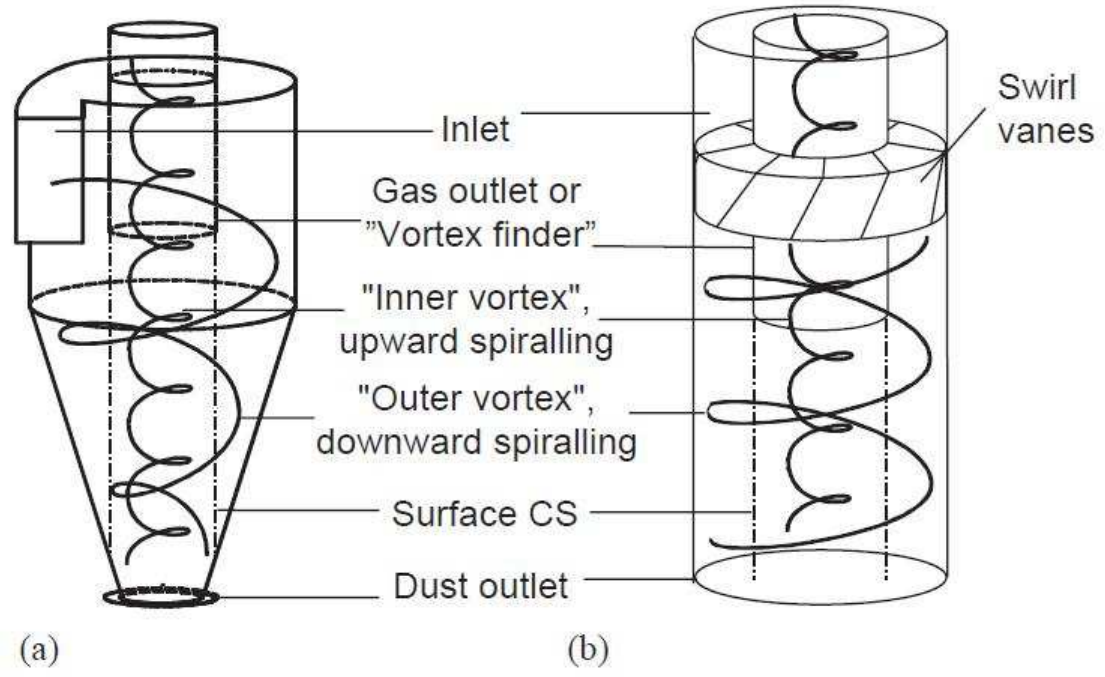

Figure 2.4: From Peng et al. [26]. Sketches of the flow pattern in a) cylinder-on-cone cyclone with a tangential inlet and b) swirl tube with axial inlet and swirl vanes.

the inner vortex. The axial velocity profile is sketched in Figure 2.5. The graph shows the outer region of downwardly directed axial flow and the inner flow of upwardly direction. The axial velocity is zero at the bottom of the cyclone before the flow reverses itself [26]. Around the centerline, the velocity in axial direction often makes a dip. This is sometimes so severe that the flow will be directed downwardly [18].

An axial inlet in the cyclone leads to a high degree of axial symmetry in the flow. This gives some advantages like eliminating the region prone to clogging on the back side of the vortex finder [18].

2.2.3 Tangential Velocity

The tangential velocity is the most important velocity profile, since the centrifugal force acts on the orbiting solid particles. The flow can be described as a Rankine vortex which has been mentioned earlier in chapter 2.1, and is a combination of the quasi-free vortex flow surrounding the quasi-forced vortex flow [26]. According to Chen [8], the tangential velocity increases with the radius and reaches a maximum at about 60-70% of the diameter before it decreases towards the wall.

The tangential velocity profile is sketched in Figure 2.6. The tangential velocity is zero at the wall and along the centerline. The value of maximum velocity is located at a

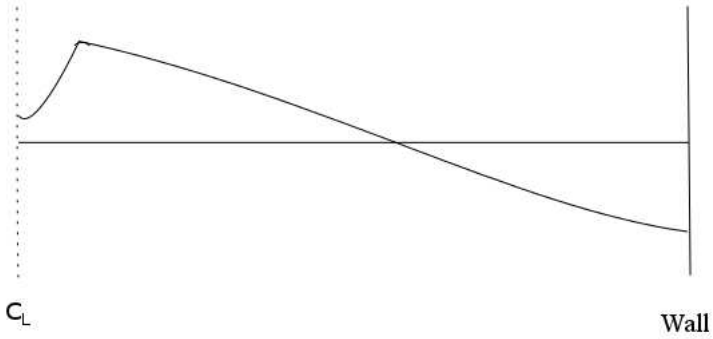

Figure 2.5: The axial velocity profile.

certain distance from the centerline represented by a radius, R_1. This radius is normally lower then the radius of the vortex finder [26].

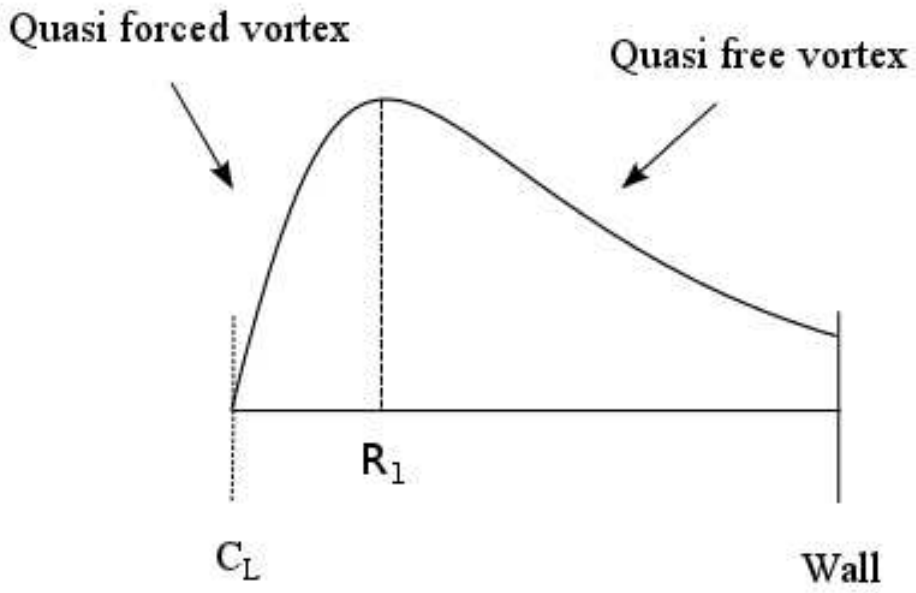

Figure 2.6: The tangential velocity profile.

2.2.4 Radial Velocity

The radial velocity is the smallest of all the three flows, and is sometimes neglected for basic calculation [26]. The flow is also more difficult to measure accurately than the

other two flows. In swirl tubes, the velocity distribution on the surface of zero axial velocity is unknown. The direction of the flow is normally inwardly and under the lip of the vortex tube. It is not uniform with height [18].

2.3 Cyclone Pressure Drop

It is necessary to understand the difference between static and dynamic pressure in cyclones. The most common way to measure the pressure drop in cyclone technology is to measure the static pressure at the wall in the upstream and downstream piping. The static and dynamic pressure can be recognized from the Bernoulli equation for a steady flow of frictional fluid. In Equation (2.4) the static pressure is referred to as p, and the dynamic pressure is $\frac{1}{2}\rho v^2$.

$$\frac{p}{\rho} + \frac{1}{2}v^2 + gh = \text{constant along a streamline} \tag{2.4}$$

From this equation, v is denoted as the gas velocity, g is the gravity, ρ is the fluid density and h is the height of the cyclone.

The static and dynamic pressure is recognized on the left side as the first and second term. The dynamic pressure is often called the velocity head. Both of them have been divided by the fluid density.

This equation shows that the static and dynamic pressures can interchange in the flow field. The area where the velocity is high, the static pressure is low. The area where the velocity is low, the static pressure is high. This principle is utilized in many types of flowmeters, for instance venturi meters.

The left side of this equation is often referred to as the Bernoulli's trinomial. In gas cyclones, the term gh is not too important compared to the two other terms, since the fluid density, ρ is relatively low, and the difference in height is not very high.

Real flows will never be frictionless, but it can be a good approximation in the outer part of a swirl in a cyclone because Bernoulli's trinomial does not change very much there [18].

The overall pressure drop includes both the static and dynamic pressure. In cyclones, this can be divided into three parts:

- loss in the inlet vanes
- loss in the separator body

- loss in the vortex finder

There is little information available for the losses in the inlet vanes on swirl tubes. If the vanes are constructed aerodynamically the losses are generally small.

The loss of pressure in the separator body are higher than for the inlet vanes. The pressures most important role is to limit the intensity of the swirl in the separation space. That means more frictional loss at the wall gives a less intensive vortex. These "wall losses" do not affect the overall pressure drop.

The part of the cyclone which has the greatest loss of pressure is the vortex finder. The losses there has an order of magnitude larger than the two other contributions. There is however one notable exception to this, and it is for highly loaded cyclones. For this case, wall losses associated with frictional drag at the walls can become a significant contribution to the pressure drop at the expense of losses in the vortex core, and the vortex finder [18].

The pressure drop in a cyclone is not easy to understand because it is being complicated by the swirling motion. The variation of the pressure drop with the geometrical and operational parameters, and the experimentally determined cyclone pressure drops, is not easy to figure out. When talking about these factors, it is important to make a clear distinction between static and dynamic pressures as mentioned above.

In the separator body, the gas moves inward from the outer to the inner part, being accelerated in accordance with the principle of conservation of moment-of-momentum of the vortex. That means that the static pressure decreases and it can be stated that the vortex transforms static pressure into dynamic pressure. Hoffmann and Stein [18] stated that "for a given wall velocity, the less the frictional loss, the more intense the vortex, the more efficient is this conversion and the lower is the central static pressure with which the gas enters the vortex finder". The cyclones that deliver the highest spin in vortex and the greatest decrease in static pressure within the core, are those that are smooth walled and aerodynamically clean.

Dissipation of mechanical energy is dependent on the friction in the walls and in the vortex core. It is this dissipation that gives a permanent pressure drop over the cyclone. An interesting fact about pressure drop in cyclones is that it decreases with increasing solid load, wall roughness or cyclone body length. These three factors give rise to an increase in the wall friction [18].

In the inlet of the cyclone the static pressure is pretty uniform over the cross section, and it is easy to measure using pressure transducers at the wall [18].

The performance of a cyclone separator is characterized by the pressure drop between the inlet and the outlet [21].

2.3.1 Euler Number

Over a cyclone, the pressure drop is almost proportional to the square of the volumetric flow rate. The dimensionless Equation (2.5) known as the Euler number gives a characteristic measure for pressure drop in a given cyclone.

$$Eu := \frac{\Delta p}{\frac{1}{2}\rho\langle v_z\rangle^2} \tag{2.5}$$

Where $\langle v_z\rangle^2$ is the mean axial velocity in the main tube.

The velocity used to define the Euler number is not important. Equation (2.5) is used a lot in research laboratories. Most engineers prefer to use the inlet velocity or the mean velocity in the vortex finder, as can be found in Equation (2.6), since most vendors and designers report these velocities in their overall performance summary.

$$Eu_{in} := \frac{\Delta p}{\frac{1}{2}\rho v_{in}^2} \qquad Eu_x := \frac{\Delta p}{\frac{1}{2}\rho v_x^2} \tag{2.6}$$

This equation is more useful for plant engineers. In their work of estimating the pressure loss through cyclones at conditions other than design conditions, or for flow rates other than the one the pressure loss is known for.

2.4 Separation Efficiency

The performance of cyclones is considered in terms of pressure drop and separation efficiency [8]. There have already been several studies performed on this theme, and this will therefore not be a concern in this thesis. However, a brief summary will be given in this section.

2.4.1 Overall Separation Efficiency

In cyclone operations there are three particle fractions to be concerned about. These are the feed, the captured or underflow and the lost/emitted particles in the overflow. Their masses are denoted with the symbols M_f, M_c and M_e and gives respectively the mass balance for solids over the cyclone:

$$M_f = M_c + M_e \tag{2.7}$$

The equation for the total efficiency, η can be calculated as the mass fraction of feed solids captured by the cyclone:

$$\eta = \frac{M_c}{M_f} = 1 - \frac{M_e}{M_f} = \frac{M_c}{M_c + M_e} \tag{2.8}$$

The efficiency of the cyclone can be calculated by collecting samples from the cyclone and weighing two of the fractions. The overall separation is normally what counts the most in an industrial process. However, it is not the best way to determine the actual separation performance of a certain cyclone since it does not say anything about the separation capability of the cyclone as a function of particle size [18].

2.4.2 Grade-Efficiency

The best way of describing the separation characteristics of a cyclone is by the grade-efficiency curve. This curve represents the separation efficiency for one particular particle size or the range of particle sizes, and it only depends on the feed density [18]. Figure 2.7 shows a sketch of a typical grade-efficiency curve. From this figure, X_{50} represents the cut size which is described further below, and x is denoted as the particle diameter.

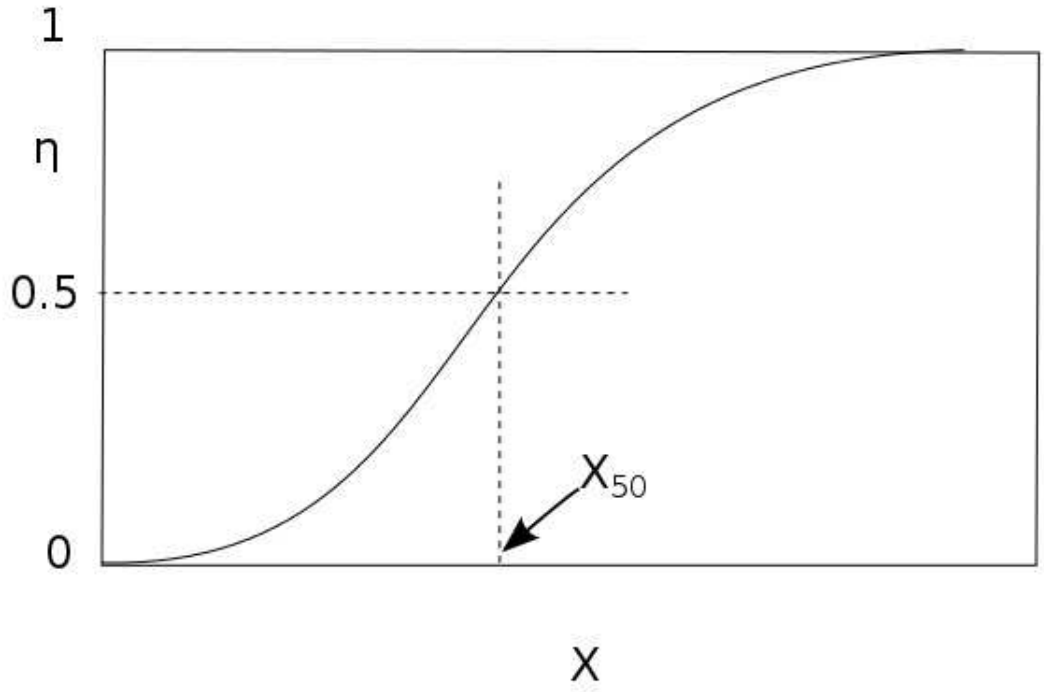

Figure 2.7: Sketch of an s-shaped grade-efficiency curve with the cut-size.

2.4.3 Cut Size

The cut size can be determined by balancing the centrifugal force and the drag force. The equilibrium of the forces can be used to determine the pressure loss, separation efficiency and operational parameters. In cyclones, particles with a diameter larger than the cut size are transported outward and separated. The particles that have a diameter size lower than the cut size are carried out through the dust hopper. This is only true in theory. In real separation, the separation efficiency curve depends on the geometrical dimensions and operation conditions in the cyclone [8].

2.5 End of the Vortex

In centrifugal separators like swirl tube and cylinder-on-cone cyclones a flow phenomenon is happening that is crucial for their performance and difficult to understand. This wellknown phenomenon is the "end of vortex" (EoV) [31]. The normal predictions in cyclone theory is that longer cyclones perform better. The best length is also significantly longer than the lengths of most available cyclones. It is known that the length of the swirl tube can not be randomly chosen. If it is made too long, the vortex will "end" spontaneously at a certain place inside the separator body [18].

Up until recently, researchers have not been able to demonstrate the exact nature of the vortex end. In literature, two different explanations among cyclone experts are circulating.

The first explanation is that the end of the vortex is an axisymmetric phenomenon, and the end is represented by some sort of recirculating gas bubble. In research of vortex breakdown in vortex tubes, the vortex end has been observed. Such a phenomenon will not occur in swirl tubes or cylinder-on-cone cyclones since it usually occurs under laminar flow conditions and the flow in cyclones are turbulent [18].

The second explanation which refer to swirl tubes and cylinder-on-cone says that the end of the vortex attaches itself to the side wall, which means that the vortex core bends off to the wall, and the vortex precesses around the wall at a high rate. This phenomenon can best be observed in cyclones using liquid where air bubbles are visualizing the end. In swirl tubes where some sort of gas is used, a small amount of powder can be injected into the tube to visualize the end of the vortex [18].

The second statement was demonstrated in laboratory by Hoffmann and Stein [18], and their conclusion is that it exists. By the use of a stroboscope under proper dust lighting conditions, they were able to freeze the motion from the precessing vortex core. They observed the EoV as it bent off and attached itself to the wall.

In the different cyclone designs, the vortex end is allowed to wander around the lower walls of the separator. The behavior and position of this end is critical to proper cyclone

performance, since it influences the efficiency, clogging and wear of cyclones operating individually or as part of a multi-cyclone installation [30].

Helmholtz continued two theorems containing the behaviour of vortices in inviscid fluids [4]:

- Vortices move with the flow of the fluid.
- The strength of a vortex tube is constant along its length.

The first theorem is pretty much self-explanatory. The second theorem says that a vortex cannot end inside the fluid, but must end up in the boundaries of the fluid or return back to form a closed path [4].

2.5.1 Factors that Affects the End of the Vortex

This section will try to enlighten the factors that affect the end of the vortex, and earlier research of the phenomenon will be looked at.

The Ring Pattern

In laboratories, the end of the vortex can be observed as a ring shaped pattern in cyclones. If air and dust are used, the formation will be observed as a dust ring on the wall. This ring defines the path of the processing vortex end. In hydrocyclones, liquid on the wall indicates the end of the vortex phenomenon. The vortex end is often marked as a dust ring or ring shaped abrasion pattern in commercial units. Two different and reasonable explanations have been suggested for the nature of the vortex end:

- The end of the vortex is an axisymmetric phenomenon and is the manifestation of an internal vortex breakdown.
- The vortex core bends to the wall of the cyclone and precesses around it to form the ring shaped pattern.

[30]

Axisymmetric Phenomenon

This phenomenon says that the main swirl would turn somewhere in the cyclone tube, and a mirror shape flow would exist underneath itself. This phenomenon was considered

by several researchers as Hoffmann et al. [17] and Qian et al. [35]. This phenomenon was later proven by Peng et al. [30] to be wrong.

Precessing Vortex

In this phenomenon, the vortex end will attach itself and precess around the lower walls inside the cyclone. The intense velocity resulting from the precessional motion of the vortex can be expected to affect the separation performance by re-entrain some of the dust collected on the bottom of the tube [19]. A sketch of a precessing vortex core is given in Figure 2.8.

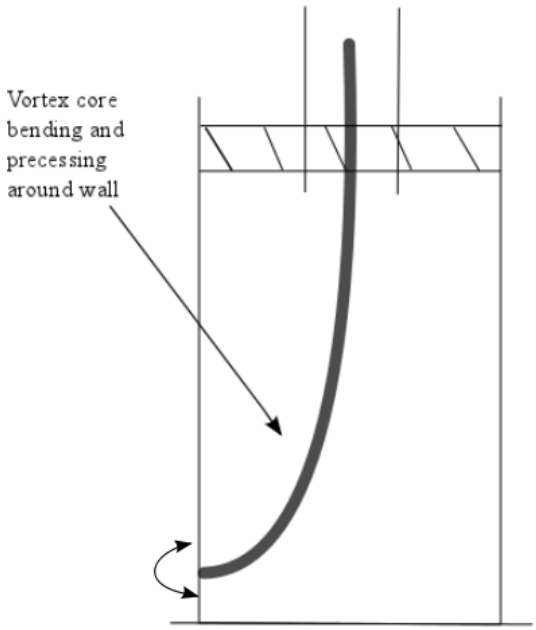

Figure 2.8: Illustration of the precessing vortex core.

Inlet Velocity

The inlet velocity for swirl tubes with swirl vanes, is not easy to determine [30]. Peng et al. [28] came up with Equation (2.9) by estimating the inlet velocity at the wall, $\nu_{\theta,w}$, by assuming uniform circumferential velocity of the gas entering from the vane pack.

$$\nu_{\theta,w} = \frac{C}{r^n} = \frac{1}{r^n}\frac{3-n}{3\pi}Q\frac{r^3 - r_o^3}{(r^2 - r_o^2)\left(r^{3-n} - r_o^{3-n}\right)\tan\phi} \tag{2.9}$$

In this equation, Q is denoted as the flow rate, r as the radius and r_o represents the outer radius.

By the use of LDA measurements on a swirl tube, Peng et al. [30] found that the swirl velocity would decrease with depth. Also by observing the behaviour as a function of

flow rate, they saw that with low flow rates without dust, the end of the vortex would form high in the tube. When the flow increased, the vortex end would move down to the bottom of the tube.

Experiments performed by Hoffmann et al. [17] showed that the dust loading had a great impact on the EoV at high inlet velocities. A high dust loading together with high inlet velocity would decrease the length of the vortex significantly. At low inlet velocities, this effect was not present.

An increase in inlet velocity will in addition to increase the vortex length also give an increase in pressure drop over the cyclone [21].

Dust Loading

As written above in chapter 2.5.1 the dust loading has an enormous impact on the swirl velocity. By inserting dust into the cyclone, the vortex stability is affected in a way that changes the apparent wall roughness. Inside the cyclone, the particles are centrifuged out towards the wall exchanging momentum with the wall through sliding or rolling and possibly leaving deposits there. The velocity will subsequently slow down, and the air underneath that region will be affected. The particles will lead to an disturbance in the outer flow similar to one would think high wall roughness would give. Therefore, the effects of charging dust is stronger at higher flow rates rather than lower since the relative velocity difference between the particles and gas are larger [16].

Geometry of the Centrifugal Separator

The different geometry configuration of cyclones affects the vortex core and its position of were the EoV attaches itself to the wall. This section will enlighten the most well known effects of the geometry on this phenomenon.

Inlet Configuration

In cyclones, the size of inlet is limited by requirements of gas handling capacity and pressure drop. Experiments have also shown that small inlet areas gives high efficiency. In cyclones with large inlet area, the vortex will bend off to the wall higher up in the separator body [1].

Swirl Vanes

The gas enters the cyclone parallel to the cyclones axis with this inlet design. A huge advantage of the axial entry is the high degree of axial symmetry in the flow. This symmetry gives operational advantages like eliminating the area prone to clogging on the back side of the vortex finder, in the area pointing opposite to the inlet opening [18].

However, It will after a short period of time quickly develop into a normal vortex flow [28].

Tangential Inlets

Since this type of inlet is the most common in use in industry most investigations have been performed on this type. The size of the inlet is of great importance to how the flow develops, and a large inlet is suitable to separate large flows, but inlets of smaller sizes give higher separation efficiency [36].

The models predicted by Bryant et al. [7] and Zhongli et al. [42] concluded that a large inlet area will increase the length of the vortex. These models are presented in chapter 2.6.1.

Separator Body

The size and length of the separator body are important factors for the position of the EoV. Previous work on this phenomenon have mostly been performed on separator tubes with a conical section [17]. Earlier investigations by Zhongli et al. [42] on similar tubes were one was built with a conical shape and the other one of cylindrical shape, gave an indication that the one with conical shape stabilizes the vortex flow better.

Tests performed by Alexander [1] on very long glass cyclones, showed that the vortex has a well defined and stable turning point inside the separator body. Even though, the length is difficult to measure since the EoV wanders up and down over a range equal to a quarter of the cyclone diameter.

Cyclones which are built slightly longer than the area of where the vortex bends off to the wall, run the full length of the vortex. It is therefore undesirable that the separator body should greatly exceed the length of the vortex [1].

According to Hoffmann et al. [17], the separation space in a cyclone is said to only be effective above the end of the vortex, and the space below the vortex end is said to be ineffective.

Vortex Finder

Zhongli et al. [42] defined the area below the vortex finder to the location where the vortex precesses against the wall, as the "natural vortex length". Because of that, the EoV is determined by the location of the vortex finder [36].

Vortex finders of different diameters have shown to have an impact on the EoV. Results from Qian et al. [36] stated that "when the diameter of the vortex finder is increased, the vortex extends deeply into the tube section initially, when the diameter of the vortex finder reaches a maximum value point, the natural vortex length has the tendency to be shorter".

The same study also indicated that the deepness of the vortex finder insertion is important. In the beginning as the deepness of vortex finder insertion was decreased, the vortex had a tendency to become longer. However, at a certain value, the vortex had a tendency to become slightly shorter [36].

Dust Hopper

Particles in a cyclone are normally collected in a dust hopper underneath the separator body [30]. The presence of the dust hopper has a great effect on the EoV phenomenon. When it is present, the swirl will suddenly move through a larger volume of gas which will normally destabilize the vortex, which again will lead to a break down [25].

Earlier investigations of the EoV phenomenon in swirl tube cyclones have shown that the vortex will in most cases bend off to the wall in the border of the hopper and the separator body. In these cases, the depth of the hopper have been an important factor. If the hopper is shallow enough, the vortex may be able to move all the way to the bottom of the hopper and centralize. In most cases when the hopper is deeper, the EoV will attach itself to the area where the hopper connects to the separator tube [32].

Hoffmann et al. [20] performed simulations on cyclones with and without a hopper section. He discovered that if he included a hopper section, the separation efficiency was higher than if the hopper was not present. The results were also closer to experimental data when a hopper section was included. In the same study he found that "The difference in predicted separation performance with and without hopper can therefore not be found in a difference in the swirl velocity".

Wall Roughness

The roughness of the wall is an important factor for the natural vortex length, and therefore also the vortex end. An important effect is that it destabilizes the vortex in cyclones. If the roughness at the wall increases, the length of the vortex decreases. Hoffmann et al. [17] found that this is often caused by the effect given by an increase in dust loading [30], [36].

The effect of wall roughness influences the tangential velocity, efficiency, cyclone separation and cyclone pressure drop for high inlet velocity [21]. Qian et al. [36] stated in his research that "the natural vortex length decreases when the wall roughness increases".

During research and experiments of the surface roughness, Kaya et al. [21] found that decreasing the tangential velocity and increasing the wall roughness in the cyclone led to an increase of the cut-size, which means a decrease in collection efficiency. The decrease in the inlet velocity also led to an increase in flow resistance and disappearance of the swirl. An excessive increase in the wall roughness led to an upward axial velocity increase in the core region. This is why the separation efficiency is exacerbated by increasing surface

roughness. At high inlet velocities, an increase in wall roughness could also cause less pressure drop [21].

Clogging and Erosion

The phenomenon where the vortex is attaching itself to the wall inside the cyclone can lead to a serious localized ring of deposits. This ring will define the path of the vortex end, and particles will settle and clog the section. The clogging can disturb the flow and significantly decrease the efficiency.

Another problem is erosion. Depending on how hard the solids are, the vortex attached to the wall inside the cyclone can lead to serious localized erosion in the form of an erosion ring. This ring can cause huge damage on the cyclone over time [17].

Cross-talk

The phenomenon cross-talk is a well known problem which occurs when swirl tubes which work in parallel, are connected to a common plenum, like a dust hopper. The phenomenon occurs when the flow is unequally distributed between the cyclone and the cyclones underflow, when they are not isolated from each other. One speaks often about "donor" tubes which happens when more gas is passing through the vanes than is exiting the separator tube, which means that it is donating gas to the dust hopper. From the "receptor" tubes, a larger amount of gas leaves the separator tube than enters through the swirl vanes. This means that gas is being pulled from the dust hopper [29].

Re-entrainment of Particles

The intense velocity from the before mentioned precession motion of the vortex end, can be expected to impact the separation performance. Some of the collected dust that is swirling down the walls can suddenly become re-entrained by the precessing vortex.

This can be a huge problem for cyclones connected to a dust hopper. If the vortex moves down to the bottom of the hopper, previously collected dust in the hopper can then be reinserted into the flow. Hoffmann et al. [17] solved this problem by installing a tube section connected between the hopper section and the separator body. The tube ended up forcing the vortex to end along its section instead.

Swirl Number

The swirl number S, is a dimensionless number which represents the axial flux of angular momentum, G_θ divided by axial flux of axial momentum, G_x times the equivalent nozzle

radius, R_x [41].

$$S = \frac{G_\theta}{G_x R_x} = \frac{\pi D_x D}{4A_i} \tag{2.10}$$

D represent the diameter of cyclone body and A_i is the inlet area.

Swirling flows result from the spiraling motion when a swirl velocity component is inserted into the inlet flow in the cyclone. Experimental studies shows that the degree of swirl imparted to the flow has large-scale effects on the flow fields [41].

Earlier studies have shown a dramatic change in the axial velocity profile of a swirling flow when the swirl numbers are altered. It is also known that the shape of tangential velocity profile does not change [41].

Swirling flows with a swirl number greater than the critical value of 0.6 in a turbulent flow induce a reverse flow in the vortex core. This will provide feedback for low frequency instabilities due to the precessing core [13].

Reynolds Number

During studies of different flows, Reynolds discovered that under some conditions, one type of flow changed to the other. He figured out that the critical velocity where laminar flow changed to turbulent flow depended on four quantities. It was the diameter of the tube, D, the viscosity, μ, the density, ρ and the average linear velocity of the fluid [23].

$$Re = \frac{\rho v D}{\mu} \tag{2.11}$$

This dimensionless group of variables is called the Reynolds number, Re. Low Re numbers below 2100 are always referred to as laminar flow in a pipe or tube. Reynolds numbers in the range 2100 to 4000, are referred to as the transition region. Under these conditions the flow can be either laminar or turbulent depending on the conditions at the entrance of the pipe or tube. Reynolds numbers above 4000 under normal conditions in a pipe or tube are always turbulent [23].

In cyclones, the inlet flow Re number increases when the frequency of the vortex core rotation increases [33].

2.6 The Natural Vortex Length

The position of the phenomenon EoV in a reverse flow cyclone, is often referred to as the "natural vortex length". It is defined as the certain axial distance from the bottom of the vortex finder to the position where the vortex attaches to the wall. The radial pressure distribution in the cyclone determines this length which is caused by the strong swirl imposed by the inlet and the location of the vortex finder [36]. Since it is known that the vortex has a natural length, one should think that it would be possible to substitute this length with the available length of the cyclone. To do this, an assumption has to be made which states that the end of the vortex limits the useful length of the separation space [19].

2.6.1 Models Predicting the length of the Natural Vortex

The natural vortex length, Ln is a parameter that has been difficult to determine experimentally [17], and during the past, only a few models have been predicted to calculate the length. In 1949, Alexander [1] made pioneering work on the subject and proposed a famous relation for the natural vortex length calculation [12].

During his research, he obtained results from tests performed on cylindrical cyclones made out of glass and came up with the following expression relating the natural vortex length where De is denoted as the diameter of the cyclone vortex finder, a is the height of the cyclone inlet and b is respectively the with of the cyclone inlet [36]:

$$\frac{Ln}{D} = 2.3\frac{De}{D}\left(\frac{D^2}{ab}\right)^{\frac{1}{3}} \tag{2.12}$$

Later Bryant et al. [7] and Zhongli et al. [42] found experimentally that Alexanders formula was not good enough to predict the length of the vortex. A formula for the vortex depth was proposed by Bryant et al. [7]:

$$\frac{Ln}{D} = 2.26\left(\frac{De}{D}\right)^{-1}\left(\frac{D^2}{ab}\right)^{-0.5} \tag{2.13}$$

and Zhongli et al. [42] figured out the following correlation:

$$\frac{Ln}{D} = 2.4\left(\frac{De}{D}\right)^{-2.25}\left(\frac{D^2}{ab}\right)^{-0.361} \tag{2.14}$$

The three equations are quite similar to each other, but the major difference in the new formulas compared with Alexander's equation are the variation of Ln. In both of the new formulas, the two dimensionless factors on the right side are opposite from Alexander's equation. The parameters that play an important role in influencing the natural vortex are the inlet velocity, cyclone length and the vortex finder insertion deepness [36].

Zhongli et al. [42] defined the natural vortex length as the distance from the bottom of the vortex finder to the dust ring. From experimental investigation, he indicated that there was a dust ring at the bottom of the cyclone with an axis width of $D/4$. From that he observed that the maximum tangential velocity of the plane where the dust ring was located was only 12% of the maximum tangential velocity at the bottom of the vortex finder. The plane with the tangential velocity profile where the dust ring was located was flat, and more than 90% of the axial velocity had been weakened [36].

Today some researchers are speculating whether these models are good enough or not to predict the natural vortex length. The predicted formulas do not include important factors like swirl number and Reynolds number for flowing fluids, and the wall roughness of the cyclone. These factors are thought to be important for predicting the natural vortex length [33].

2.7 Computational Fluid Dynamics

Computational fluid dynamics (CFD) uses numerical methods and algorithms to solve and analyze problems that involve fluid flows. To perform the calculations required, computers are used to simulate the interaction of liquids and gases with surfaces defined by boundary conditions [22]. During recent years, numerical investigations have been performed on cyclone separators for determination of their characteristics and it has proven to be a promising tool for investigation [3].

2.7.1 Background and History

CFD has been in use since the beginning of the 1970s, and one of the first simulations of the flow in an industrial cyclone was performed already in 1982 [6]. Since the beginning, the simulations have gone through a dramatical change. The computers that existed at that time and the algorithms, limited all practical solutions essentially to two-dimensional flows. Compressors, turbines, flow ducts and similar equipment are in the real world three-dimensional. The speed capacity and the storage of the computers did not allow CFD to operate in any practical way in this three-dimensional world. Today simulation of three-dimensional flow fields are more or less an industrial standard. The development of faster computers with more memory, has resulted in its use as a tool in the design process [2].

CFD is only meant to complement pure theory and experiments and will never replace either of them [2]. Chen [8] stated in his master thesis "CFD simulations, at the current level of development are primarily a tool for understanding the important features of a system and for predicting trends for scale-up purposes."

All of CFD is based on the fundamental governing equations of fluid dynamics; the continuity, momentum, and energy equations. The physical principles of fluid dynamics are based on these three equations [2]:

- mass is conserved
- Newtons second law, F = ma
- energy is conserved

2.7.2 Turbulence Models

In practice, most flows are turbulent and therefore need special treatment. Turbulent flows are three-dimensional and time dependent. For people who are unfamiliar with this phenomenon, a plot of velocity as a function of time at different points in the flow would look pretty random and chaotic. The turbulence makes the conserved quantities stirred which means that parcels of fluid with different concentrations of at least one conserved properties are brought into contact. This is often called turbulent diffusion. Fluids of differing momentum content which are brought into contact is caused by turbulence. The kinetic energy of the flow is reduced according to the reduction of the velocity gradients due to the action of viscosity. The lost energy is irreversibly converted into the internal energy of the fluid. Another important property of turbulent flows, is that they contain coherent structures which are responsible for a large part of the mixing. The random component of the turbulent flows causes these events to differ from each other in size, strength and time interval. This makes the study of them very difficult. Turbulent flows fluctuate on a broad range of length and time scales. These are all important factors to turbulent flows [11].

A huge problem with the use of CFD are that most gas flows in cyclones are turbulent. One would think that if the computational grid could be made fine enough, CFD could solve the fundamental equations directly and that the turbulence would occur automatically in simulations. This is not possible in real process equipment, and turbulence models are required to minimize the turbulence on the mean gas flow pattern [18].

A short introduction to the most common methods of simulating turbulent flows are presented in this thesis.

Reynolds-Averaged Navier-Stokes models

Reynolds-Average Navier-Stokes (RANS) equations offers many turbulence models for investigating the mean properties of turbulent flows. Two of these models are the Reynold Stress model and Eddy viscosity model which are mentioned under. This turbulence model are also the oldest approach [38].

Reynolds Stress Models

The Reynolds Stress model (RSM) is the turbulence model used in simulations for this thesis and it gives an accurate prediction of the swirl flow pattern. The turbulence model simulates the axial velocity, tangential velocity and pressure drop in the cyclone [39]. The model calculates the individual Reynolds stresses directly by solving their governing transport equations [38]. The model is able to predict complex flows more accurately than other models like κ - ε because it accounts automatically for the effects of stress anisotropy. Because of this, it simulates the cyclone flow well. However, several terms in the exact Reynolds Stress transport equations are unknown and model assumptions based on simple flow observations have to be introduced to close the set of equations [6], [8].

RSM solves the Reynolds stresses, $\rho\overline{u_i' u_j'}$ and the transport equation is written as

$$\frac{\partial}{\partial t}\left(\rho\overline{u_i' u_j'}\right) + C_{ij} - D_{ij} = P_{ij} + \Phi_{ij} - \rho\varepsilon_{ij} \tag{2.15}$$

where C_{ij} is the convection term, D_{ij} is the diffusion term, P_{ij} is referred to as the generation or production term, Φ_{ij} is the pressure-strain term, and $\rho\varepsilon_{ij}$ is the dissipation term [38].

Eddy Viscosity Models (κ - ε)

This model has on its basic form a major advantage in its simplicity and practical usability. Zhou and Soo [43] used the κ - ε in their work of improving the performance of the cyclone separator. Their project used this model for solving the tangential and axial velocity. In their work they discovered that it had a limitation in the near axis region, where the numerical prediction gave higher values than those obtained from measurements. The κ - ε model can not account for the non-isotropic turbulent structure due to the different magnitudes of velocity components. In turn, this has shown that high values of magnitudes of turbulent viscosity leads to higher axial velocity near the axis [8].

This turbulence model is useless for the cases of highly swirling flows because the assumption of isotropy [6].

Large Eddy Simulation

Large Eddy Simulations (LES) is a mathematical model suited for modeling complex flow phenomenon by predicting the motion of the large structures in the turbulent fluid flow [22]. The high computational intensity compared to RANS simulations made LES simulations less suited for the daily CFD applications when it was first published [10]. With the improving technology of computers in recent years, this model has had an enormous impact in CFD since it reduces the empiricism involved [31].

LES is usually the preferred method for flows with higher Reynolds number, or if the geometry is too complex for DNS to handle [11]. This turbulence model involves computation of the large-scale turbulent motions which are responsible for the turbulent mixing [31].

Direct Numerical Simulation

Direct Numerical Simulation (DNS) provides very detailed information of the flow. It is the most accurate approach in turbulence simulations since it calculates the Navier-Stokes equation without averaging or approximation other than numerical discretization. The error can be estimated and controlled, and is probably the simplest approach. In DNS, all of the motions included in the flow are resolved [11].

A valid simulation captures all of the kinetic energy dissipation. This happens on the smallest scales where the viscosity is active, and because of that one will need a very fine grid. The size of grid can not be larger than a viscously determined scale called the Kolmogorov scale, η.

This turbulence way of simulating is limited by the speed and memory of computers and can only be carried out for flows with low Reynolds numbers and simple constructions. Flows containing high Reynolds number and larger geometries will need another turbulent approach for simulations.

2.7.3 Modelling of Wall Friction

The wall roughness should be taken into account in the law of the wall since it leads to a change in the velocity profile of the boundary layer.

In CFD simulations, the wall roughness is modelled in the following way.

The velocity distribution near the wall is modeled as:

$$u^+ = \frac{1}{\kappa} \ln \left(E^{'} y^+ \right) \tag{2.16}$$

where κ is von Karman constant and has a default value of 0.42. The parameter y^+ represents the non-dimensional wall coordinate, and the wall function coefficient $E^{'}$ is given as:

$$E^{'} = \frac{E}{f} \tag{2.17}$$

For tubes with smooth walls, the default value of $E = 9$, and the friction function f is unity. The friction function also modifies the log-law coefficient E which again is a function of the roughness parameter:

$$R^+ = \frac{r_h u_\tau}{\nu} \tag{2.18}$$

r_h is represented as the equivalent sand-grain roughness height and u_τ is the friction velocity. The value of f are given as:

$$f = \begin{cases} 1 & \text{for } \mathrm{R}^+ \leq \mathrm{R}^+_{\text{smooth}} \\ \left[B\left(\frac{R^+ - R^+_{smooth}}{R^+_{rough} - R^+_{smooth}}\right) + CR^+\right]^a & \text{for } \mathrm{R}^+_{\text{smooth}} < \mathrm{R}^+ < \mathrm{R}^+_{\text{rough}} \\ B + CR^+ & \text{for } \mathrm{R}^+ > \mathrm{R}^+_{\text{rough}} \end{cases} \tag{2.19}$$

where the exponent a is expressed as:

$$a = \sin\left(\frac{\pi}{2}\frac{\log\left[R^+/R^+_{smooth}\right]}{\log\left[R^+_{rough}/R^+_{smooth}\right]}\right) \tag{2.20}$$

The default coefficients values are: $B{=}\,0$, $C{=}\,0.253$, $R^+_{smooth}{=}\,2.25$ and $R^+_{rough}{=}\,90$ [33].

Chapter 3

Literature survey

3.1 End of the Vortex

During the past decades, several investigations of the flow field and cyclone performance in centrifugal separators have been well reported in literature. The behaviour of the phenomenon known as end of the vortex in swirl tubes has not been given too much focus, and there are still many unanswered questions. Most of the studies performed in this field have been on cyclones shaped like cylinder-on-cone. Some of these studies are mentioned in this section.

3.1.1 Alexander [1949] [1]

In this study, Alexander performed pioneering work, and came up with the first model to predict the natural vortex length. In his work, he investigated the nature of the gas flow within a cyclone under varying conditions of operations. The pressure drop was investigated along with the velocity profile and the angles of flow within the barrel.

3.1.2 Hoffmann et al. [1995] [17]

In this study, they measure the position of the vortex end by the use of two different types of cyclones. One cyclone made out of glass and one made out of metal. Both cyclones had a tube section underneath the conical section to connect the dust hoppers at the bottom.

During this study, two experimental methods for determining the natural vortex length by detecting the vortex end were performed. For the first method they inserted smoke, consisting of paraffin oil, into the cyclone made out of glass. When doing this, they

observed that there is very little interchange of gas between the region over and under the end of the vortex. They also used dust in the glass cyclone so that they could observe the position of the end of the vortex.

For the second method, they used dust in the metal cyclone to measure the pattern of wall deposits on the walls. This pattern was created by the vortex end, and after every run they had to open the cyclone to measure it.

3.1.3 Peng et al. [2005] [30]

This study uses a stroboscope and high time resolution pressure measurements to visualize the EoV phenomenon in cylinder-on-cone cyclones and swirl tubes. Peng discovered that the end of the vortex occurred higher in the swirl tube when the solid loading increased and the flow rate was decreased.

By the use of a strobe-light he was able to "freeze" the vortex end when the dust ring appeared in the separator, and he observed a small circular pattern of dust at the wall. He concluded that the vortex phenomenon in swirl tubes is due to the vortex bending to the wall and ending there, and not because of the break-down of the vortex internally in the fluid. He concluded his study by saying that "controlling the end of vortex is necessary to improve operational characteristics further".

3.1.4 Cuizhi et al. [2010] [12]

In this study, pressure measurements are used to prove the existence of the EoV phenomenon in a cylindrical dipleg. A cylinder-on-cone cyclone is used for performance of the experiments.

By the use of Fast Fourier Transform (FFT) and probability density analyses of wall pressure, they identified the EoV behaviour at the point of attachment in the cyclone.

3.1.5 Pisarev et al. [2010] [31]

In this study, Pisarev performed several numerical tests using CFD simulations. He performed simulations on different lengths of separator bodies, and he looked at the EoV phenomenon with the presence and absence of a dust hopper. By the use of LES simulations, he discovered that the inlet velocity was an important factor for the EoV phenomenon. He figured out that when the vortex core bent to the wall of the separator, the time-mean of the axial position of attachment was not constant in time. He described the behavior of the vortex core as a function of the length of the tube.

3.1.6 Pisarev et al. [2011] [32]

In this study, different CFD models of swirl tube cyclones were built to study the EoV phenomenon. By the use of LES turbulence model, Pisarev performed several measurements on cyclones with variable length of separator body. He discovered that in some cases the vortex would bend to the wall and rotate around it before it went down along the body and centralized. In other cases he found that the vortex would bend to the wall and precess around it, and that it would remain there.

He also found that the depth of the dust hopper was an important characteristic for the EoV phenomenon. In swirl tubes cyclones containing dust hoppers underneath, the vortex would bend off to the wall at the position where the separator body connects to the dust hopper. This was the case for all inlet velocities. The vortex would only centralize for dust hoppers with the smallest size of depth.

3.2 Wall Roughness

The effect of wall roughness in cyclones has not yet been studied extensively, so little research material is available.

3.2.1 Kaya et al. [2011] [21]

This study investigates the effects of surface roughness on the flow field in a tangential inlet cyclone. The study is carried out using numerical simulations, where Reynolds Stress turbulence model is used to solve the governing equations of the gas flow. Kaya compared the results from numerical simulations with results from experimental data and mathematical models. He figured out that if he increased the relative roughness on the inner walls of the cyclone, the tangential velocity, cyclone separation efficiency, and cyclone pressure drop was influent considerably for high inlet velocities.

Chapter 4

Experimental Setup and Numerical Boundaries Conditions

4.1 Description of the Swirl Tube and its Equipment used in the Experiments

The experiments were carried out using a experimental test rig. The overall layout is sketched in Figure 4.1. Pure air at ambient condition is supplied to the experimental rig from a centrifugal pump. This pump is located in the downstream of the separator and air is drawn through the system by depressurisation at the outlet. To adjust the flow rate, two control valves are used. For changing the main flow, the flow valve is used, and for fine-tuning of the flow, the bypass valve is used. The design of the separator body is cylindrical and, according to Pisarev et al. [31] this shape reduces the uncertainty caused by the geometry when it comes to the fundamental study of the EoV phenomenon.

The figure shows that the gas flows horizontally into the tube and then changes to a vertical direction. To mitigate the flow before reaching the swirl vanes, three baffles were installed so that the flow would be distributed better over the annular cross-section.

The swirl tube consists of three distinct constructions:

- separator body
- swirl vanes
- vortex finder

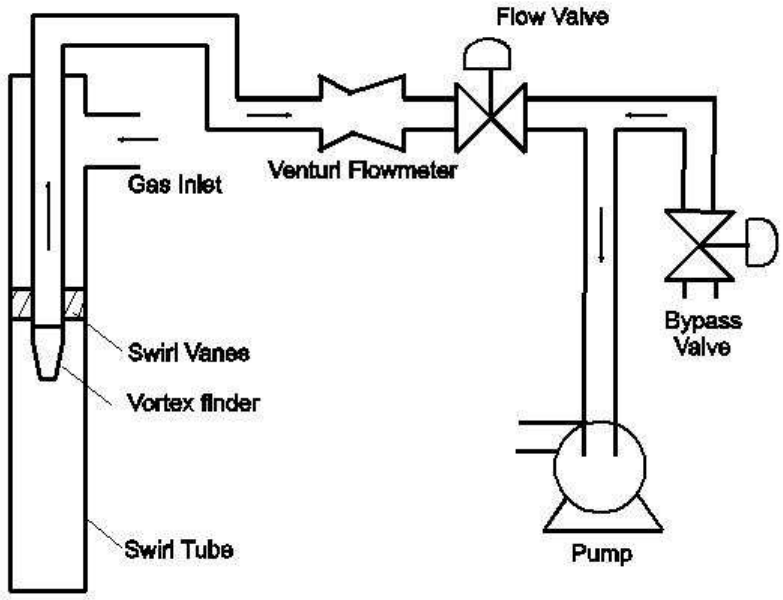

Figure 4.1: The experimental setup of the test rig.

4.1.1 The Separator Body

The separator body is a cylindrical shaped tube constructed of transparent plexiglas. The separator is transparent which makes the flow phenomena inside the tube easier to observe. For the smooth tubes, the inner surface roughness is estimated to be less than 1μm, which is quite smooth.

The dimensions and a picture of the separator body can be seen in Figure 4.2. The length of the separator body is an important factor when it comes to bending of the vortex phenomenon.The lengths used in the experimental rig were respectively 70 cm, 90 cm and 110 cm, and is referred as X cm in the sketch. The diameters of the tubes used in the experiments were 10 cm over the entire length.

Because of the simple construction of the separator, no dustbin or dust outlet was connected to the tube. The intention of this was to reduce the effect of the geometry on how the vortex end would behave. This caused all the particles captured in the air inside the tube to gather on the bottom piece. For industry, this design will have no practical value since it would be difficult to get the collected particles out of the separator. When more particles are put into the tube, the concentration at the bottom will increase and it can cause re-entrainment and change of apparent roughness.

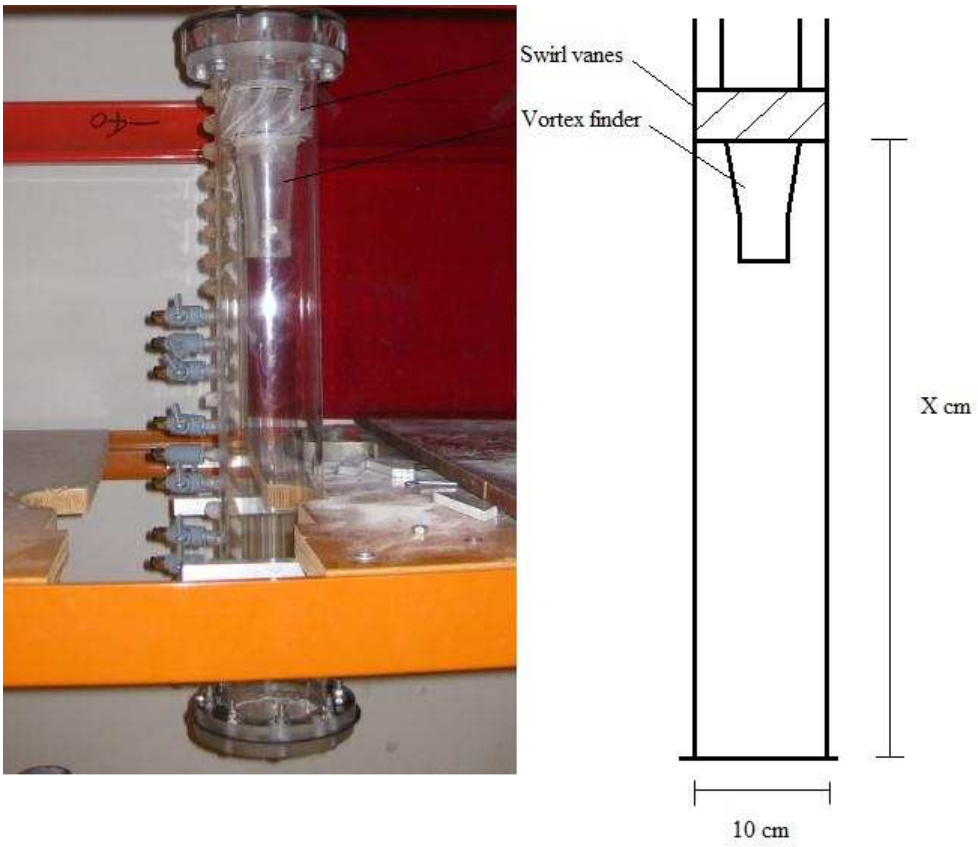

Figure 4.2: A picture and a sketch of the separator body.

4.1.2 Swirl Vanes

A sketch with the dimensions of the swirl vanes, and a picture of the swirl vanes are shown in Figure 4.3.

The swirl vanes in the inlet of the main body of the separator give the tangential component. The velocity is higher at this point than anywhere else in the tube, because the vane pack represents the lowest cross-sectional area, even though the flow is still assumed to change quickly from uniform flow to a more Rankine-vortex type of flow pattern below the vanes. The most important characteristic of the swirl vanes is the exit angle, which was 30° to the horizontal plane [31]. The flow in axial direction, ν_z is given by

$$\nu_z = V_{in} \cdot \sin(30°) = \frac{1}{2} V_{in} \tag{4.1}$$

for the flow exiting the swirl vanes. In this equation, V_{in} represents the inlet velocity. The flow in tangential direction ν_θ below the swirl vanes is given by

$$\nu_\theta = V_{in} \cdot \cos(30°) = \frac{\sqrt{3}}{2} V_{in} \tag{4.2}$$

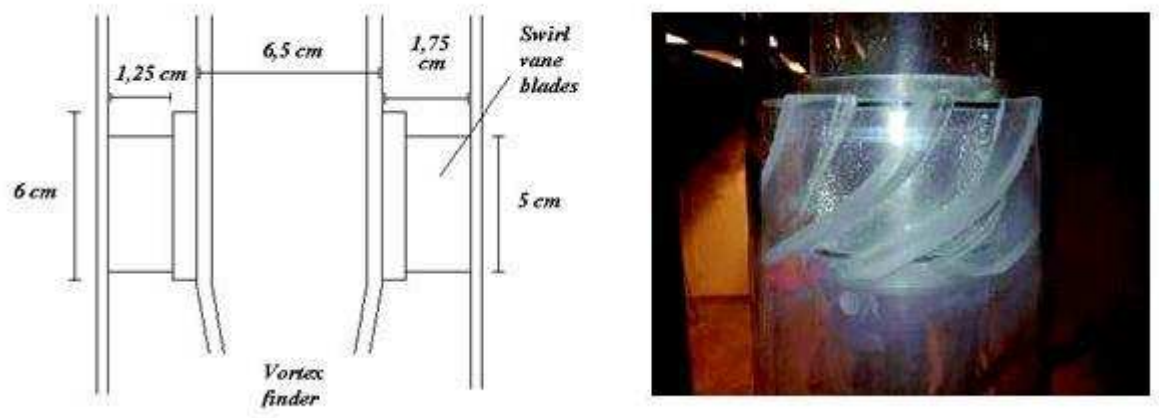

Figure 4.3: From Pisarev et al. [31]. An illustration including the dimensions and a picture of the swirl vanes.

4.1.3 Vortex Finder

The diameter and shape of the vortex finder are important dimensions in determining the end of the vortex phenomenon [30]. In literature it is found that by increasing the diameter of the vortex finder, the natural vortex length has a tendency to become shorter [36]. The diameter is also the most important factor in deciding the separation efficiency and pressure drop in cyclones [31]. The dimensions and a picture of the vortex finder from the test rig are given in Figure 4.4. The size plays a critical role in defining the flow field inside the cyclone, including the pattern of the outer and inner spiral flows [37].

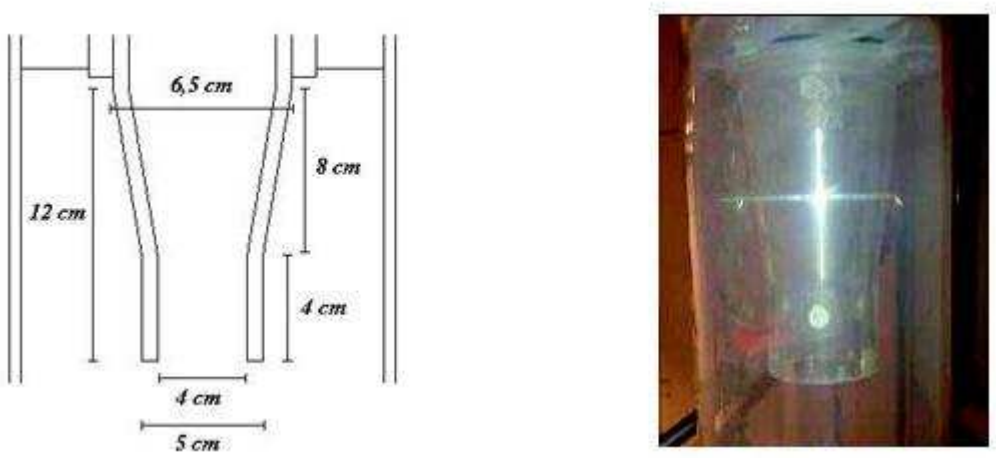

Figure 4.4: From Pisarev et al. [31]. An illustration including the dimensions and a picture of the vortex finder.

The vortex finder at the test rig is of conical shape below the swirl vanes, and has a 4 cm cylindrical section at its end. This allows us to study the EoV at a moderately narrow

relative vortex finder diameter De/D of 0,4 where De is denoted as the diameter of the vortex finder and D is the diameter of the cyclone body.

4.1.4 Pressure Transducers and Tappings

A pressure transducer is a transducer that converts pressure into an analog electrical signal. They are locating and following the rotation frequency of a swirl, by monitoring the wall pressure using a series of pressure tappings on the separator body. A picture of the pressure transducer is given in Figure 4.5. The transducers are connected to an interface box which again gives the measured values to a computer.

Figure 4.5: A picture of a pressure transducer.

The pressure tappings are arranged in axial rows on the walls of the swirl tube body, which are shown in Figure 4.6. There are 22 tappings on the 70 cm tube, 26 tappings on the 90 cm tube and 35 tappings on the 110 cm tube. The distance between each tapping is 3 cm and is the same for all tubes. The last tap is located 3 cm from the bottom of the swirl tube body. The tapping diameter is 0.5 mm, which is small enough to avoid disturbance of the flow but still big enough to get an adequate fast response time. The pressure tappings are actually small valves. A tube from the pressure transducer can be connected to the end of the valves and the measured values will be sent to a computer for registration.

Figure 4.6: The pressure tappings on the separator body.

4.1.5 Wall Roughness

The wall roughness may be an important factor to the EoV phenomenon. In order to make the inner walls of the separator tube rough, two different ways of treating the walls was performed:

- Sanding the walls with sandpaper.
- Coating the walls with metal particles.

To make the inner walls of the separator tube rough, sandpaper with particles of 0.8 mm in diameter was used to roughened the tube on the inside. The hight of the roughness was measured in a microscope after particles generated from the sanding had been collected. The roughness is estimated to be between $100 - 120\mu m$.

In the second method, coating the inner walls with metal particles gave a uniform layer of surface roughness over the entire separator tube. The inside of the tubes was sprayed with glue and metal particles were placed inside. The tube was locked in both ends and then shaken until the particles covered the hole section. When the glue had dried, the superfluous particles were removed. A picture of the tube covered with metal particles is given in Figure 4.7. The roughness was estimated to be between $180 - 200\mu m$.

Figure 4.7: The separator tube covered with metal particles.

4.2 Performance of the Experiments on the Swirl Tube

4.2.1 Measurement of the Flow Rate

The flow rate, Q, is an important factor when it comes to where the end of the vortex bends off to the wall, and it has to be measured quite precisely. A digital venturi flowmeter is used since it is important to have an accurate instrument to measure this. The venturi measures the difference in pressure. For the characteristic and the equations of the venturi flowmeter, see Appendix A.

The pressure transducers are connected to two tubes. One tube is connected to the pipe right before the venturi flowmeter, and the other one is connected to the neck of the venturi. The difference in pressure between these two points is measured and the value is given in voltage. The value 43.75 mbar, or 4375 Pa corresponds to an increase of 1 V. The difference in pressure, Δp is found by calculating the difference between the measured voltage and the voltage at no flow.

$$\Delta p = (U_{measured} - U_0) \cdot 43.73 \cdot 100 \tag{4.3}$$

The parameter U_0 is referred to as the pressure difference when there is no pressure corresponding to no flow in the tube. This value is normally around 1 V, but before every new measurement, it had to be measured for variation inside the system. The pressure transducers can measure a difference up to 5 V, which is 175 mbar or 17,5 KPa.

The commercial software program LabView, is used to read and calculate the measured value from the pressure transducers. During measurements of the flow rate, samples are taken for 10 seconds with a sample rate of 100 s^{-1} and 1000 s^{-1} for a total of 1000 and 10000 voltage values. The measured values are averaged before Equation (4.3) is used to calculate the difference in pressure, which in turn are used to calculate the flow rate.

$$Q = \frac{C_d A_2}{\sqrt{1 - \left(\frac{A_2}{A_1}\right)^2}} \sqrt{\frac{2\left(P_1 - P_2\right)}{\rho}} \cdot 3600 \tag{4.4}$$

To calculate the flow rate into inlet velocity, v_{in}, the cross-sectional area of the inlet must be known. The diameter of the pipe is 8,0 cm, and the diameter at the neck is 4,2 cm. The cross-sectional area give us $A_1 = 5.02 \cdot 10^{-3}$ m^3 and $A_2 = 1.39 \cdot 10^{-3}$ m^3 respectively. In order to find the inlet area, the axial position to measure it must be defined. The vortex finder has a conical shape and the annular area of the inlet region increases as it goes down from the swirl vanes down to the bottom of the vortex finder. The area at the lower section is defined as the inlet area since we can assume the flow to develop into the same flow pattern at the bottom as for a straight one. The outer diameter of the vortex finder is found to be 5 cm and the diameter of the swirl tube is 10 cm gives an inlet area of

$$A_i = \frac{\pi}{4}\left(D^2 - De^2\right) = 5.9 \cdot 10^{-3} m^2 \tag{4.5}$$

The inlet velocity at a given flow rate could be found from the Equation (4.6) below.

$$v_{in} = \frac{Q}{A_i \cdot 3600} \tag{4.6}$$

4.2.2 Observation of the Flow with Dust Injected

The easiest way of detecting the vortex inside the tube is by visualizing the flow. The separator tube is made out of transparent plexiglass, so it is easy to observe the flow inside. By watching the flow inside closely we can see the shape of the vortex, and how it performs in the system. Any change in behaviour can be observed and is valuable information for research.

Since we are dealing with pure air, the vortex can only be visible if dust or other substances are injected into the system. During the performance of the experiments, two different ways of injecting the particles were used:

- A small amount of fine dust was inserted at the bottom of the tube. When the vortex reached the bottom it became visibly apparent.

- A large amount of fine dust was inserted at the gas inlet on the top. The vortex became visible as it went downward and its length and shades could be detected.

The amount was kept as low as possible to avoid too much of an effect on the clean air, since it is known that dust affects the vortex flow. Another important reason to keep the amount of dust low, was to protect the pump since it did not have any filters or other equipment to prevent any damage to it. On the few occasions where a large amount of dust was injected into the system, the behaviour of the vortex, and how it differed from the other experiments containing low concentrations of dust, was observed.

4.2.3 Measurement with Pressure Transducers

The pressure transducer was connected to the tappings at the separator body to measured the frequency with which the vortex core rotates in the swirl tube. This method detect the end of vortex and is performed to measure the exact position were the vortex bends to the wall, and precesses around the wall which was observed. Figure 4.8 shows a sketch of how the vortex core passes a measurement point and how the pressure tapping is capturing the pressure drop.

The static pressure is reduced and the velocity at the end of the vortex is higher than in the air outside. When the vortex core spins around the separator, continuous measurements at points along the wall will detect a drop in pressure when the vortex flows very close by.

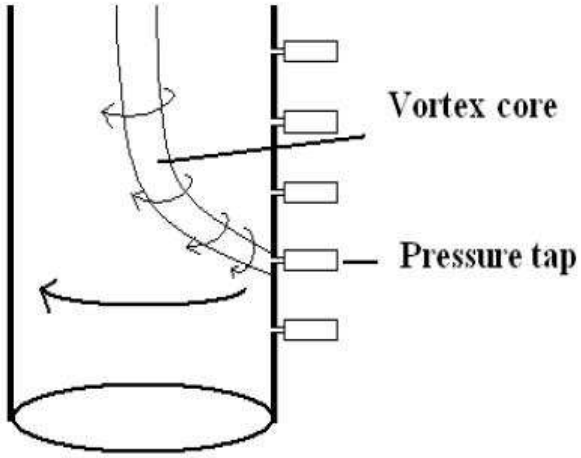

Figure 4.8: From Gjerde [16]. A sketch of the vortex core passing the pressure tappings while it is bending to the wall and precessing around it.

4.3 Computational Setup

4.3.1 Software and Simulation Preference

The software used for simulation is the commercial CFD software STAR-CD, v4.08 from CD-Adapco. The program was developed for the calculation of fluid flow, heat and mass transfer and chemical reaction in industrial and environmental applications. It also provides a large number of available options for the solving of the flow, like the different solution algorithms, wall boundary treatments and turbulence models. The model grid could also easily be built within the program [38]. The whole swirl tube was taken into account. The model's geometry and operational variables in simulations were built to match the configuration on the experimental test rig. This included the shape of the swirl vanes, the vortex finder and the baffles. The commercial program Star Design was used to built the model. The meshing was performed using Star-CCM+ to ensure that the calculations was made accurate at the important areas such as the boundaries. Figure 4.9 gives an overview of the model.

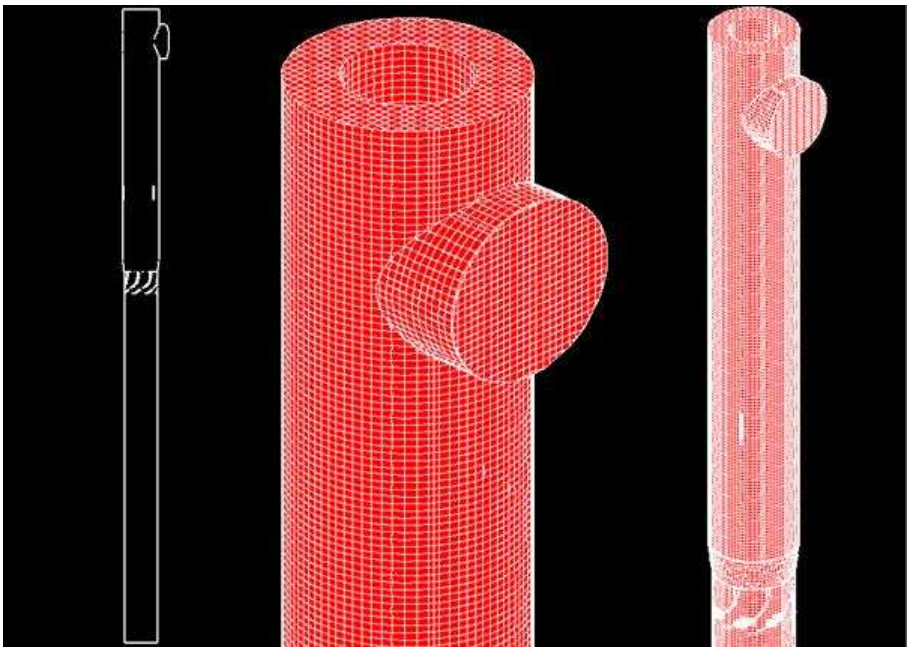

Figure 4.9: From Pisarev et al. [31]. An overview of the CFD model. The figure on the left shows the complete geometry of the model on the inside, including the edges of the swirl vanes, baffles and the inlet. The figure in the center shows the horizontal inlet into the tube section. On the right side, the figure gives the entire upper section of the model.

In present work, the numerical grids consist of about 172000 cells, and have a cell size of 4 mm. The grids were built in a cylindrical coordinate system. The gravity force was directed along the z-axis so it would coincide with the axis of the separator. Grid refinements tests have been performed in order to make sure that the solution is not grid dependent.

The experiments were carried out at the following conditions. The working fluid was pure air with constant density of 1.205 kg/m^3, molecular viscosity $1.81{\cdot}10^{-5}$ Pa and molecular mass 28.96 kg/kmol. The temperature was set to be 293 K. The angle of the incoming gas in the swirl tube was 45^o in all cases.

The Reynolds Stress model was chosen because several bodies of research assert that this model is suitable for these type of simulations [31], [35], [40]. The Gibson and Launder model was used to compute particle motions.

For the inlet boundary conditions, the inlet velocity was varied between 20 m/s and 60 m/s and was placed at the gas inlet of the separator. Pressure boundary condition was also set at the inlet and was set equal to atmospheric pressure. A negative inlet at the outflow surface was prescribed and a no-slip boundary condition was used on the solid wall boundaries. In order to change the roughness in the simulations, the ELOG parameter at the wall was adjusted between 1,2 and 2. The simulations were carried out on one cylindrical tube with length of 60 cm.

The SIMPLE algorithm was chosen for discretization. This is a solution that uses an iteration strategy method. It works in a way that it first predict one value and then correct this value in the next iteration. The flow equations are temporarily decoupled from each other and solved continuously. Following, this was used for the pressure-velocity coupling in order to accelerate the convergence by combining of the continuity equation. A transient run was performed, using the steady-state results for initial conditions with five iterations for each time step. Time steps of 0.001 s and a total simulation time of 20 s were used.

A general problem using a detailed 3-D model in CFD is the huge amount of computational cells necessary to run the simulations. In this case, simulations of 1 s took about 7 hours.

Chapter 5

Results and Discussion

This chapter is divided into three general topics:

- Comparison with earlier work on the project.
- Measurement with pressure transducers.
- Measurements on a swirl tube containing rough wall surface.

The results from each part is analyzed and discussed separately in every section.

5.1 Comparison With Earlier Work on the Project

The tests were performed using two different methods of dust injection. For the first method, a small amount of dust was injected into the bottom of a clean tube, so it would be possible to see the shape of the vortex through the tube. Since only a small amount of dust was injected into the bottom, the vortex would not be affected on its way down to the bottom, but it could only be located in the bottom of the tube once it had centralized.

The other method was injecting a large amount of dust into the top of the tube. This method made it possible to locate the vortex all the way down to the bottom of the tube and it was possible to see the swirling motion, where it attached itself to the wall, formed and centralized on the bottom. This method was only used for locating the position of where the vortex attached itself to the wall, and not for determining the flow rate at which the vortex centralized. This is done because it is stated in literature that insertion of particles has been found to decrease the stability of the vortex as written in chapter 2.5.1. The temperature in the room was the same for all experiments and was around 293 K

Chapter 5.1 provide tables showing different values of flow rate needed for centralization at variable lengths of separator bodies. Graphs comparing new results versus old ones are shown for each length of tubes. A graph summarizing the values of centralization is given in the end of this section. Tables containing all the experimental measurements are given in Appendix B. Some of the present results will be compared with earlier results obtained by Gjerde in swirl tubes that were constructed from segments joined by flanges with rubber O-rings [16]. Even though the joints at that time were made to fit as well as possible the concern in these early experiments remained that the disturbance due to the joints influenced the behaviour of the vortex end. It had also been observed that the vortex end seemed preferentially to precess at positions a few cm above these joints.

5.1.1 60 cm Swirl Tube

This was the shortest tube that was used for experimental tests. By injecting a huge amount of particles into the top, one could observe that, upon formation, the vortex core bent and attached itself to the wall, around 39 cm below the swirl vanes. When a small amount of dust was added to the bottom of the tube, the vortex was, as mentioned only visible when it reached the bottom and centralized. Table 5.1 shows the results. For the lowest flow rate below 39 m^3/h the tests were run for about 2 minutes, but the vortex did not centralize. For a flow rate over 39 m^3/h the vortex core first attached itself to the wall, but after a while moved down to the bottom and centralized. For the highest flow rate, 66.2 m^3/h, it appeared that the vortex centralized immediately.

Before every single test, the zero-flow rate was measured, since it has a tendency to vary a bit during the day. The electronic readout from the flowmeter varied for the zero-flow between 1.0351 and 1.0422, which gives a small difference for the lower flow rates. Between every measurement, the centrifugal pump was shut down for at least 15 minutes before the next run. This was done to be sure that there was no residual flow left in the tube, so that the next test would not be affected.

The measured values from the 60 cm separator tube are compared to earlier tests by Gjerde on the same experimental rig. His testing is from a configuration of two tubes with different lengths connected together, a 35+20 cm. Those results showed that the vortex core centralized for a flow rate around 52.5 m^3/h.

The results from Figure 5.1 show that the flow rate from the tube configuration of 60 cm centralizes for lower values than it did for the 35+20 cm (55 cm) configuration. The difference can of course be the 5 cm difference in tubes, but, as mentioned, visual observation in connection with earlier measurements have given rise to the belief that it is because of the joints between the two tubes.

Configuration [cm]	Flow rate [m^3/h]	Comments
60	39.4	NC
	39.7	C in 35 seconds
	39.8	C in 23 seconds
	40.2	C in 20 seconds
	40.9	C in 20 seconds
	41.5	C in 19 seconds
	66.2	C in 1.5 seconds

Table 5.1: Measurement of the flow rate in a 60 cm tube with smooth walls. NC means not centralized, and C stands for centralized.

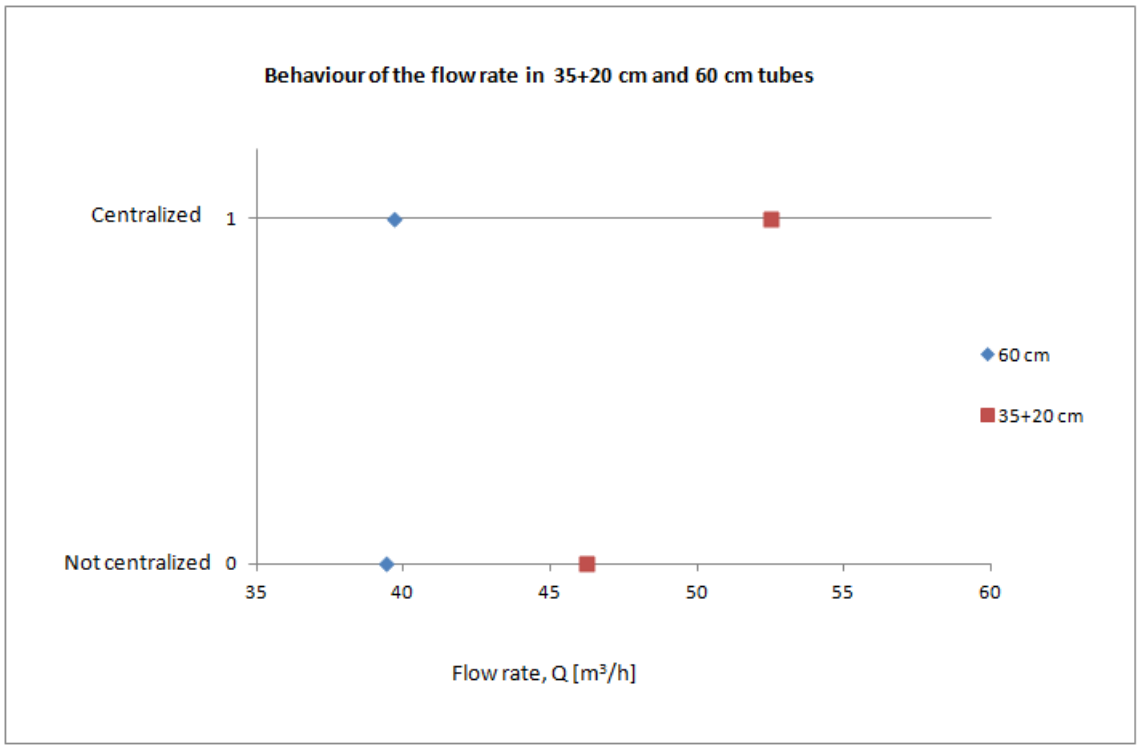

Figure 5.1: A plot giving a comparison of the results from an 35+20 and 60 cm separator tube. The plot shows for which flow rate the vortex bends off to the wall and does not centralize and the lowest value were it is centralized.

5.1.2 80 cm Swirl Tube

For this length of tube the vortex core attached itself to the wall at about 65 cm below the swirl vanes, when a large amount of particles were injected into the top of the tube. Judging by visual observation at the bottom with only a small amount of dust injected, the vortex did not centralize for values lower than 56 m^3/h. For the flow rates over 56 m^3/h, the vortex core bent to the wall initially, upon formation, before it went down and centralized at the bottom. The results are listed in Table 5.2.

The results from the 80 cm swirl tube are comparable to two earlier results from tubes with configuration of 35+40 cm and 35+50 cm.

Configuration [cm]	Flow rate [m^3/h]	Comments
80	50.3	NC
	56.6	C after 51.6 seconds
	67.3	C after 15.5 seconds
	78.0	C immediately

Table 5.2: Measurement of the flow rate in a 80 cm tube with smooth walls.

The new measurements show that the flow rates centralize for lower values than it did for the earlier measurements. There is still a 5 cm difference in tube lengths for the new tube compared to the old tubes with connections. This can lead to a bad picture of the results. The new tests give a centralized flow with a flow rate around 56 m^3/h. The old tests from a 35+40 (75 cm) configuration give a centralized flow around 56 m^3/h, and the tests from the 35+50 (85 cm) configuration give a centralized flow at 70 m^3/h.

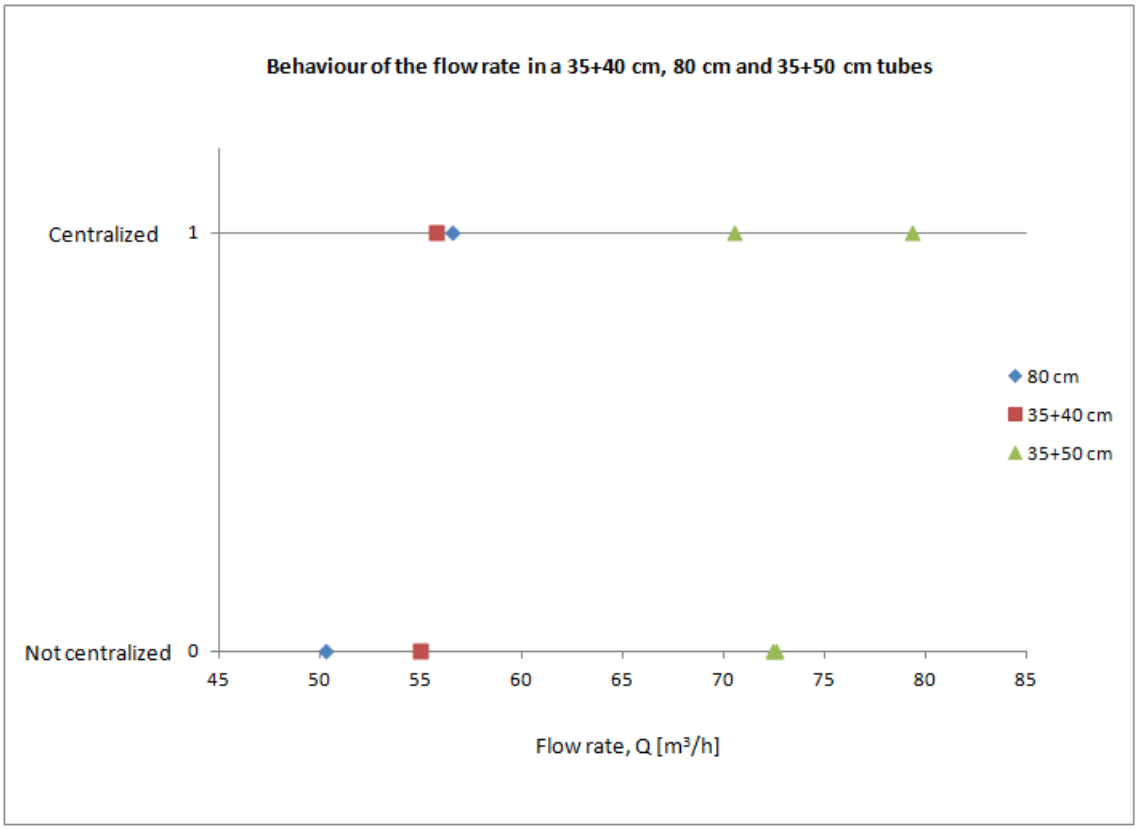

Figure 5.2: A plot giving a comparison of the results from an 35+40 cm, 80 cm and 35+50 cm tube. The plot shows whether the vortex bends off to the wall or if it is centralized.

The results given in the plot in Figure 5.2 give a good picture of which flow rate is needed to achieve a centralized vortex in these tubes. A strange result from the earlier measurements is the centralized flow rate value of 70.5 m^3/h in the 85 cm tube. The first

thoughts on those results are that something is incorrect with the measurements since the flow rates of 72.4 m^3/h and 72.6 m^3/h which are higher than the first centralized flow rate of 70.5 m^3/h do not centralize but bend off to the wall instead. The vortex does not centralize again until it reaches the flow rate 79.3 m^3/h.

5.1.3 100 cm Swirl Tube

This was the longest tube used for the experimental test. For this length of tube the vortex core attached itself to the wall at about 82 cm below the swirl vanes, when a large amount of particles were injected into the top of the tube. As can be seen from the values in Table 5.3, the vortex core did not centralize for values of flow rates lower than 90 m^3/h. For these values it only bends to the wall. For values of flow rate higher than 90 m^3/h, the vortex core bends at first to the wall and forms before it goes down to the bottom and becomes centralized.

The measured values from the 100 cm swirl tube given in Table 5.3 are compared to earlier tests with a configuration of three tubes with different lengths connected together, a 35+40+20 cm (95) tube configuration.

Configuration [cm]	**Flow rate [m^3/h]**	**Comments**
100	85.2	NC
	90.2	C in 45 seconds
	111.5	C in 12 seconds

Table 5.3: Measurement of the flow rate in a 100 cm tube with smooth walls.

These results show that in a 100 cm tube the vortex centralizes for flow rates of around 90 m^3/h in the new measurements. For the 35+40+20 cm tube from the old experiments, the vortex core centralized at around 116 m^3/h. These values tells that the results from the new measurements deviate from the old measurements in the same way as they did for the 60 and 80 cm tubes. The deviation of 5 cm in tube lengths is still present for these measurements as well as it were for the previous measurements for the 60 and 80 tubes.

The plot in Figure 5.3 gives a good picture of which values of flow rate the vortices are centralizing at. It can easily be seen that the vortex in the 100 cm tube is centralizing for much lower values of flow rate than it does for the configuration of the 35+40+20 (95) cm tube.

Figure 5.4 gives a graph showing where the different lengths of tubes have their centralizing flow rates. Two lines represents the curves where the blue line with three measurements points shows the new experiments on the new tubes. The red line with four points represents the old experiments on the old tubes with two or three segments.

The results done on the new swirl tubes compared to the old results, give a clear picture that the new configuration with only one tube as a whole, centralizes the vortex for lower

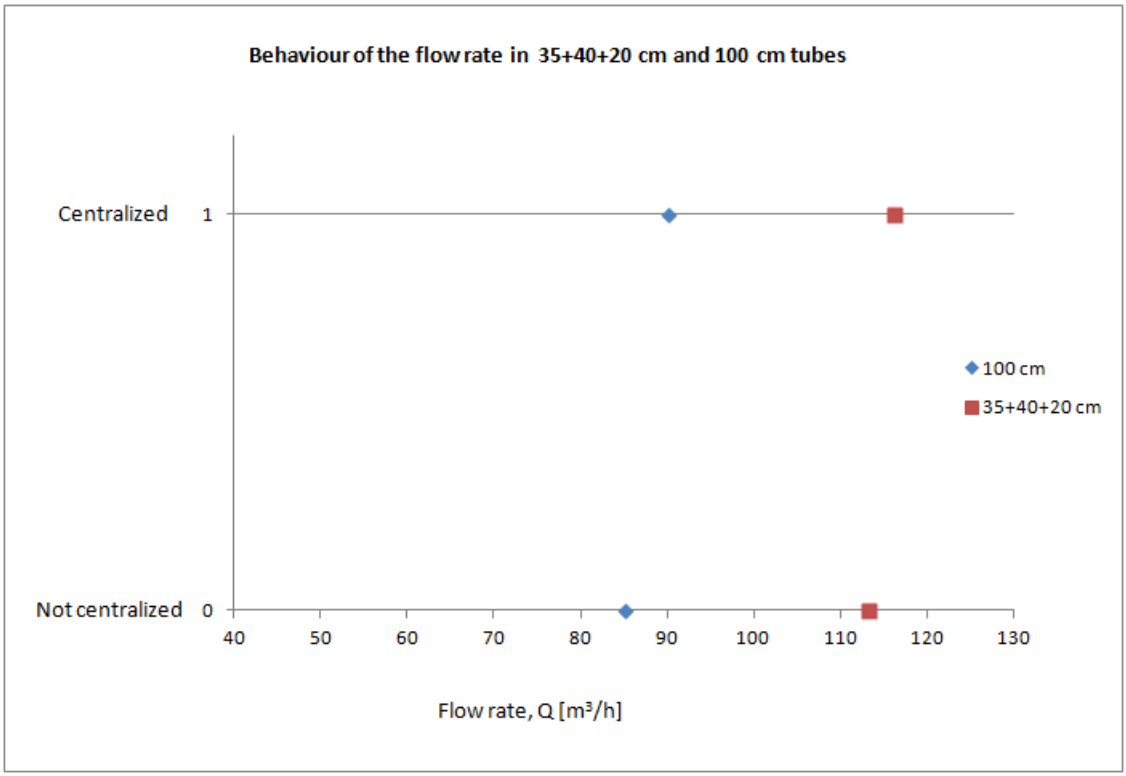

Figure 5.3: A plot showing the comparison of the results from an 35+40+20 cm and 100 cm tube. The plot shows whether the vortex bends off to the wall or if it is centralized.

values than was the case for tubes with more than one configuration. A conclusion to be taken from these results is that the joints between the configurations on the tube affects the vortex, and needs a higher flow rate to centralize at the bottom of the tube. The values of the flow rates and the different lengths of the tubes are both important factors. The results show that longer tubes need higher flow rate before centralization.

A small problem which may occur by injecting too many particles into the tube is that the wall roughness can be changed. This might result in the vortex core taking a different path on its way down the tube, and give bad results for the next measurement. The effect of wall roughness was not wanted in these results, so the tube was occasionally cleaned between the measurements.

During the experiments, the centrifugal pump had to be shut down for at least 15 minutes between every measurement to give accurate values. If the pump was started too early, an residual flow would still be left inside the tube and affect the results by centralizing the flow at low values of flow rate that should theoretically be impossible. The flow rate at these values was checked several times when the pump had been off long enough and the results showed that it would never centralize at those low flow rates.

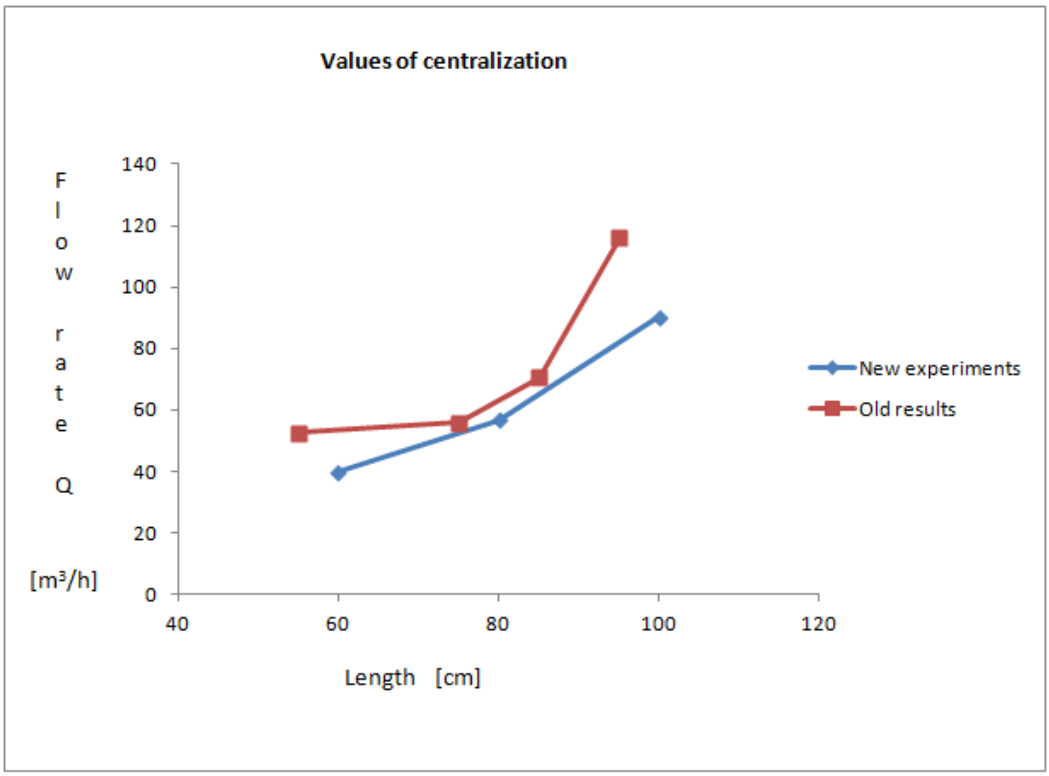

Figure 5.4: A graph showing the values of centralization from the different tubes compared to the old experiments.

5.1.4 Standard Deviation of the Flow Rate from the Centrifugal Pump

To be able to figure out the standard deviation of the pump, several measurements were carried out on the experimental test rig without changing the flow rate at the valves. A table containing all measurements is given in Appendix C.

The variance from the measurements gave:

$$s^2 = \frac{\sum_{i=1}^{n}(x_i - \overline{x})^2}{n-1} = 4.88 \text{ m}^3/\text{h}$$

and the standard deviation became:

$$s = \sqrt{\frac{\sum_{i=1}^{n}(x_i - \overline{x})^2}{n-1}} = 2.21\text{m}^3/\text{h}$$

The standard deviation is a quite large.

The uncertainty of the standard deviation can be found from:

$$s_s = \frac{s}{\sqrt{2(n-1)}} = 0.78$$

Because of the high standard deviation, the zero flow rate was accurately determined

before starting the centrifugal pump. This was performed for every new running experiment to be sure that this uncertainty did not have to be taken into account.

5.2 Measurement with Pressure Transducers

On the separator body, pressure tappings were connected to pressure transducers over the length of the separator body in axial direction. They were connected to measure the frequency with which the vortex core rotates, inside the body of the swirl tube. This measurements was performed for each length of separator tube at different flow rates. This method detect the end of vortex and is performed to measure the exact position were the vortex bends to the wall and precesses around it. The reason for performing these measurements was to find out if it would bend to the wall at the same place independently of the flow rate which have been a crucial assumption in the models predicting the position of the vortex end used throughout research and industry. The pressure transducers were used to measure the pressure at different positions on the wall at the same flow rate during start up. The pressure plugs on the tube were placed at a distance 3 cm apart. The time period measured was 10 seconds including 1 to 3 seconds before start up of the centrifugal pump.

Results and pictures from each measurement for tubes of 80 and 100 cm can be found in Appendix D.

The figures from LabView gives two different pressure curves. The white curve is pressure measured with a high resolution pressure transducer on different places on the tube. The red curve is pressure measured on the inlet flow and is not important in these measurements. The pressure curves in the figures from LabView are traced upside-down so it looks like the wall pressure is higher after the vortex hit the wall, but it is actually lower.

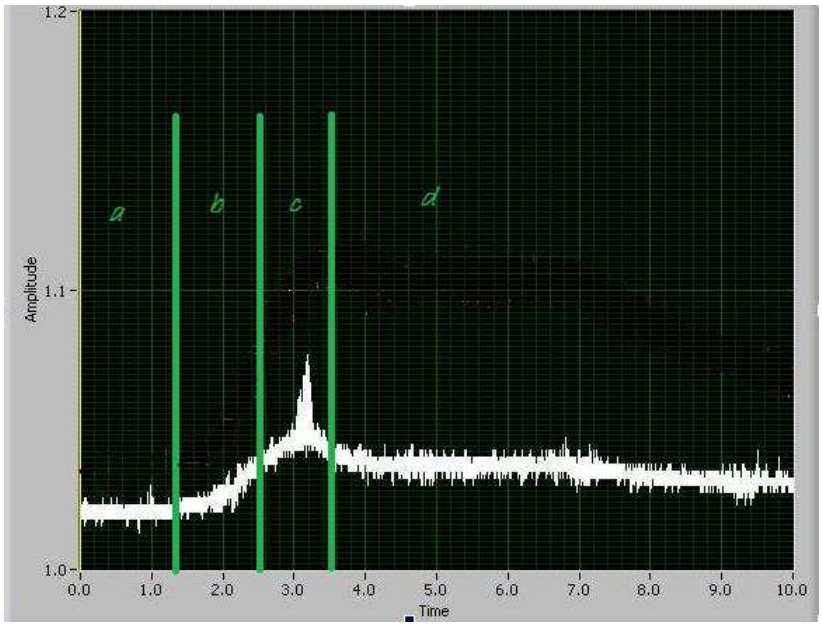

Figure 5.5: The pressure profile of the end of the vortex in a swirl tube, measured with pressure transducers.

The print screen picture in Figure 5.5 gives a pressure profile inside the swirl tube on the downward moving vortex end. The picture is divided into section from a) to d). Section a) represents the pressure at a given time in the tube before start-up of the centrifugal pump. The area in b) shows the profile of the pressure before the EoV passes the tapping. In section c), the vortex end is passing the tapping, and the figure gives a characteristic drop or trough in the wall pressure. Section d) shows the pressure profile after the vortex end has passed the tapping and moves down to the bottom before centralization. The jumps in the figure has to do with the limited resolution of the pressure transducers.

60 cm Swirl Tube

The 60 cm swirl tube was measured at three different flow rates to see if the vortex would bend and form at the same place independently from the flow rates during the start up of the centrifugal pump. It has been stated in literature that an increase in gas velocity will give an increase in pressure drop in a cyclone as written in chapter 2.5.1.

Flow rate of 173 m^3/h

Table 5.4 gives en overview over the occurrences if the sudden drops in wall pressure in the tube. It shows the location were the EoV bends to the wall before it moves down and centralizes for flow rates of 173 m^3/h in a 60 cm tube.

Distance from swirl vanes [cm]	Comments
56	Pressure trough after 2.5 seconds
44	Pressure trough after 2.5 seconds
35	Pressure trough after 2.5 seconds
32	Pressure trough after 2.5 seconds
29	No pressure fall

Table 5.4: Measurement of the pressure trough in the swirl tube immediately after start up in a 60 cm tube with pressure transducers. Q = 173 m^3/h.

Immediately after start-up of the pump, at a flow rate of 173 m^3/h, there is no difference in pressure, and the vortex end has not yet attached to the wall, as the flow is passing the tap. This is shown in Figure 5.6. Figure 5.7 shows a jump in the pressure after about 3.6 seconds which means a pressure drop has occurred. It is at this point the EoV is passing the pressure tap, and the pressure profile shows that the pressure are lower after the vortex end has passed by. It can be seen that the position where the vortex attaches itself to the wall and precess around it, the wall pressure will undergo a sudden and significant decrease. From these results, it can be seen that the flow bends to the wall somewhere between 29 cm and 32 cm from the swirl vanes.

The flow rate at 102 m^3/h

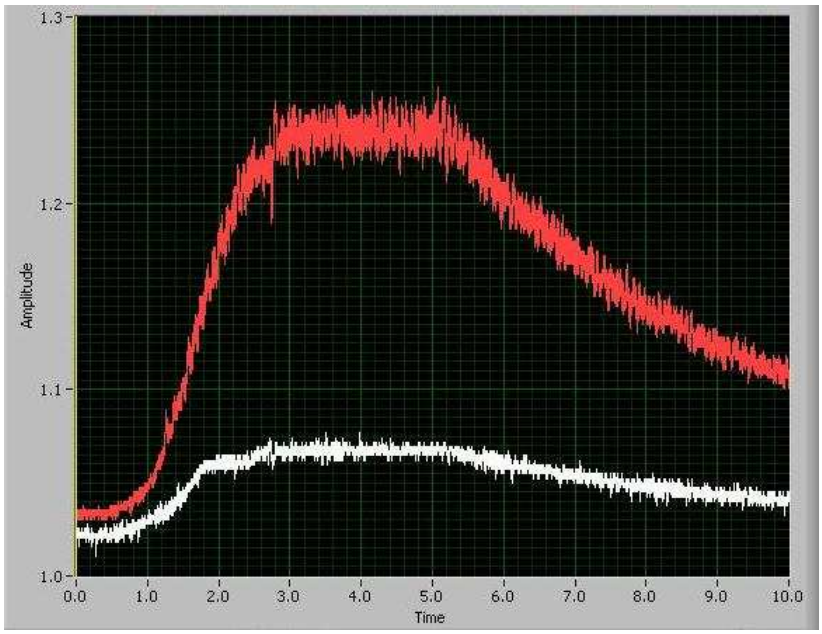

Figure 5.6: Output from LabView. Q = 173 m^3/h. Pressure measured at a point 29 cm from the swirl vanes in a 60 cm tube.

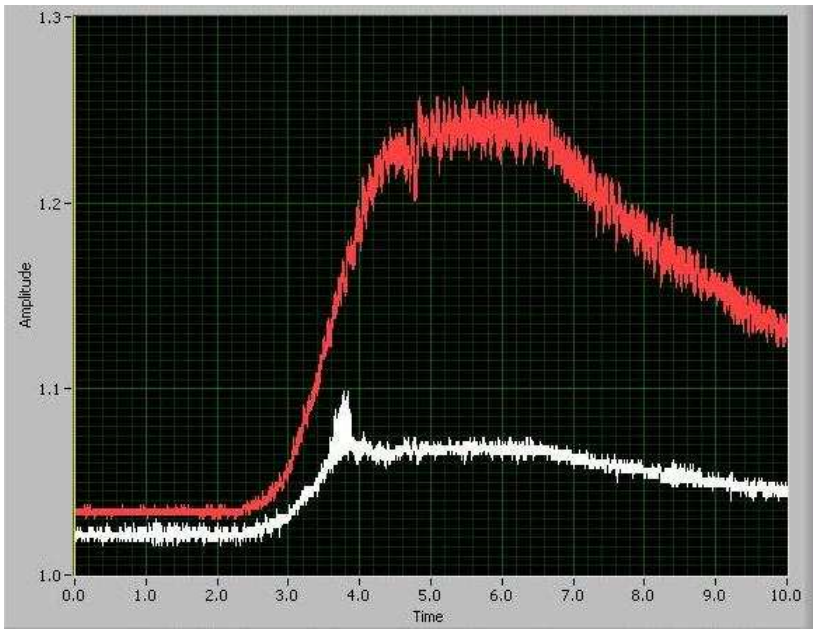

Figure 5.7: Output from LabView. Q = 173 m^3/h. Pressure measured at a point 32 cm from the swirl vanes in a 60 cm tube.

Table 5.5 gives en overview over the pressure trough in the tube. It shows the location were the EoV bends to the wall before it moves down and centralizes for flow rates of 102 m^3/h in a 60 cm tube.

Distance from swirl vanes [cm]	**Comments**
44	Pressure trough after 2 seconds
41	Pressure trough after 2 seconds
35	Pressure trough after 2 seconds
32	Pressure trough after 1.5 seconds
29	No pressure fall

Table 5.5: Measurement of the pressure trough in the swirl tube immediately after start up in a 60 cm tube with pressure transducers. Q = 102 m^3/h.

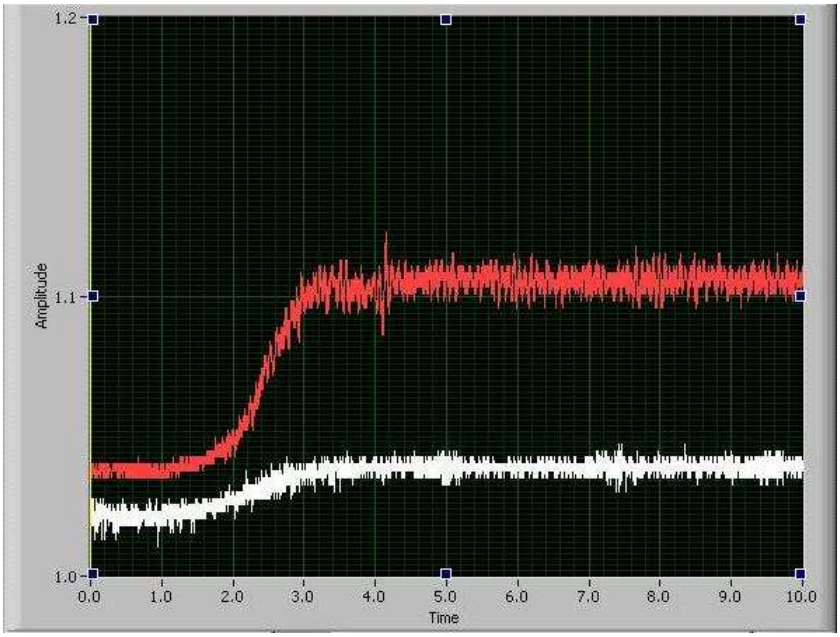

Figure 5.8: Output from LabView. Q = 102 m^3/h. Pressure measured at a point 29 cm from the swirl vanes in a 60 cm tube.

From Figure 5.8 and 5.9 it can be seen that the position of the core is still in between 29 cm and 32 cm from the swirl vanes. Since Figure 5.8 shows little difference on the pressure curve over time, and Figure 5.9 gives a picture of a jump in the pressure curve about 1 seconds after start up.

Flow rate of 72.8 m^3/h

Table 5.6 gives an overview over the pressure trough in the tube. It shows the location where the EoV first occurs on the wall before the vortex core moves down and centralizes for flow rates of 72.8 m^3/h in a 60 cm tube.

With the flow rate at 72.8 m^3/h in Figure 5.10 and 5.11 it can still be seen that there

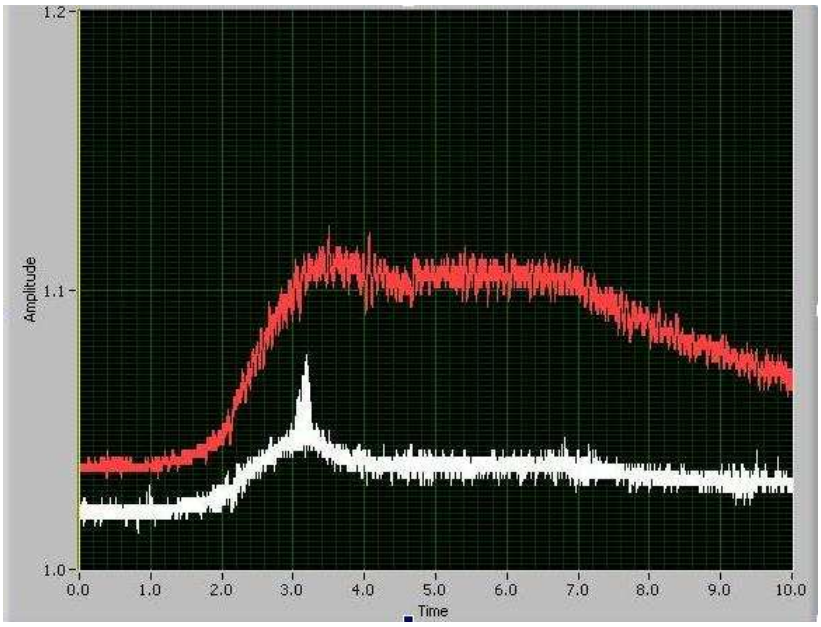

Figure 5.9: Output from LabView. Q = 102 m^3/h. Pressure measured at a point 32 cm from the swirl vanes in a 60 cm tube.

Distance from swirl vanes [cm]	**Comments**
41	Pressure trough 2.5 seconds
35	Pressure trough after 3 seconds
32	Pressure trough after 3 seconds
29	No pressure fall

Table 5.6: Measurement of the pressure trough in the swirl tube immediately after start up in a 60 cm tube with pressure transducers. Q = 72.8 m^3/h.

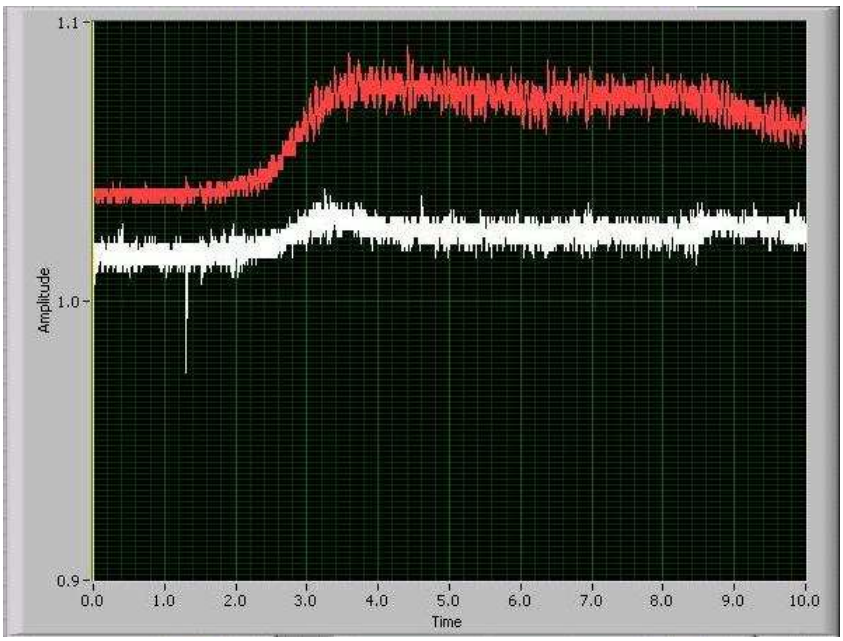

Figure 5.10: Output from LabView. Q = 72.8 m^3/h. Pressure measured at a point 29 cm from the swirl vanes in a 60 cm tube.

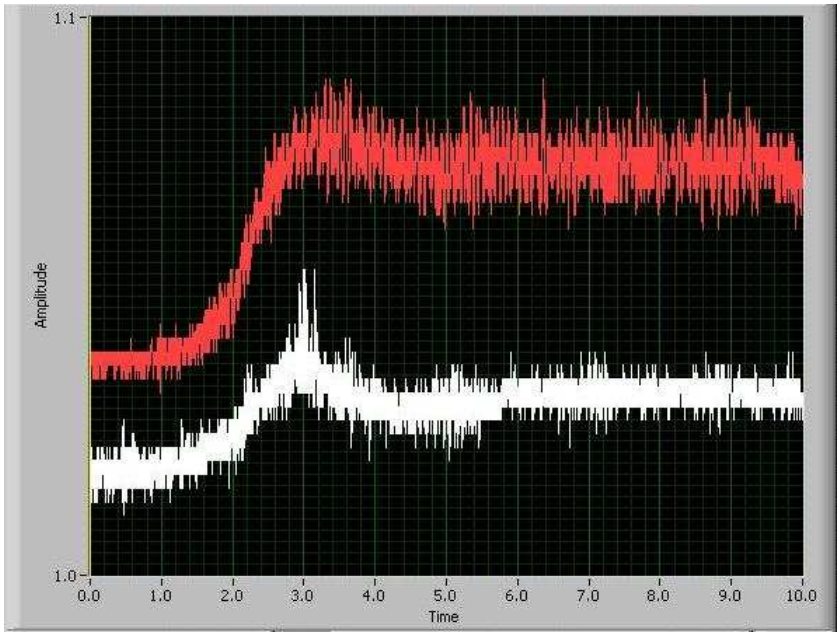

Figure 5.11: Output from LabView. Q = 72.8 m^3/h. Pressure measured at a point 32 cm from the swirl vanes in a 60 cm tube.

is a pressure jump 32 cm from the swirl vanes, but no one in the figure 29 cm from the swirl vanes.

These results can indicate that for a 60 cm swirl tube the vortex bends to the wall independently of the value of the flow rate during start up.

80 cm Swirl Tube

The flow rate at 67 m^3/h

The time before the vortex became centralized was about 17 seconds. Table 5.7 shows the location where the vortex core bends to the wall by the use of pressure transducers for flow rates of 67 m^3/h in a 80 cm tube.

Distance from swirl vanes [cm]	Comments
34	Pressure trough after 4 seconds
28	No pressure fall

Table 5.7: Measurement of the pressure trough in the swirl tube immediately after start up in a 80 cm tube with pressure transducers. Q = 67 m^3/h.

The flow rate at 156.6 m^3/h

The time before the vortex centralized was about 3 seconds. Table 5.8 shows the location were the EoV bends off to the wall by the use of pressure transducers for flow rates of 156.6 m^3/h in a 80 cm tube.

Distance from swirl vanes [cm]	Comments
34	Pressure trough after 4 seconds
28	No pressure fall

Table 5.8: Measurement of the pressure trough in the swirl tube immediately after start up in a 80 cm tube with pressure transducers. Q = 156.6 m^3/h.

For these lengths, the pressure tapping located 31 cm below the swirl vanes was sadly broken. Therefore measurements had to be performed on the next one available, which where located 34 cm below the swirl vanes.

The results from this length of tube indicated the same as for the 60 cm tube. The vortex bended off somewhere in between the area of 28 cm to 34 cm below the swirl vanes.

100 cm Swirl Tube

The flow rate at 111.5 m^3/h

The time before the vortex centralized was about 12 seconds. Table 5.9 shows the location were the EoV bends off to the wall by the use of pressure transducers for flow rates of 111.5 m^3/h in a 100 cm tube.

Distance from swirl vanes [cm]	Comments
31	Pressure trough after 2 seconds
28	No pressure fall

Table 5.9: Measurement of the pressure trough in the swirl tube immediately after start up in a 100 cm tube with pressure transducers. Q = 111.5 m^3/h.

The results shows the same phenomenon for all the cases independently of the difference in length and flow rate. From these present results it can be thought that the bending of the vortex can be a start up phenomenon.

The results shows that the bending of the vortex happens some place in between 29 to 31 cm below the swirl vanes. This is the case for all lengths independently of each others flow rate.

Earlier research by Peng et al. [30] have proven that when the vortex core moves around inside the tube, the flowmeter detects a small peak for every 5 measurement points. In Pisarev et al. [31] a similar study showed a small peak for every 22 measurements points. The reason these peaks exist is due to the low pressure in the vortex, and is detected every time the vortex is passing the flowmeter. It has also proven to be regular in time, but not in depth. The same results appeared in these present measurements where the peaks from the output pictures are irregular in depth.

From the same study by Peng et al, a popping noise was identified every time the low pressure in the core passed the pressure tapping. In the present study, the same noise was identified during the performance of the experimental measurements.

5.3 Measurements on a Swirl Tube with Varying Wall Roughness

Experiments on the inner surface roughness were performed on two sizes of separator tubes, 60 and 80 cm. The tubes were the exact same tubes used in earlier experiments with smooth surface. These lengths were chosen because earlier investigations from Pisarev et al. [31] have shown that these lengths are suitable for these type of measurements. The 80 cm separator tube was treated by two different ways to achieve the roughness inside that was wanted to get sufficient measurement results. The first was roughening the walls by the use of sandpaper, and the second was coating the walls with metal particles of known size.

This section provides tables containing flow rates at which the vortex centralizes at, and graphs showing the values of flow rate where it centralizes at.

The last part shows pictures from numerical simulations of the pressure profiles from the vortex flow.

5.3.1 Walls Treated with Sandpaper.

The walls on the separator tubes were roughened up with a sandpaper with particles of 0.8 mm in diameter. The final height of the roughness on the wall was estimated to be approximately 0.1 - 0.2 mm, and was found by collecting the wall dust which appeared when the sandpaper roughening of the separator tube found place. The dust was observed in a microscope and the size was estimated. The estimating part was performed by PhD candidate G. Pisarev.

The experimental procedure was the same as for the cyclone with smooth walls.

The results from these measurements showed a slight difference in the time at which the various events took place, but not so much in the flow rate. The flow rate needed for centralization for the cases where the separator body was 60 cm were approximately 39.7 m^3/h. For the ones with 80 cm separator body, the flow rate required for centralization were 58 ± 2 m^3/h for both cases.

The values given in Table 5.10 are measurements performed on swirl tubes of 60 and 80 cm. Experiments were first run on the tubes while their surface were still smooth. Afterwards, the tubes were roughened up with sandpaper so the inner walls contained a rough surface.

Results from these tubes did not differ too much compared to results from the smooth tube. It was predicted that the vortex core would bend off to the wall further up in the tube, and that it would need a larger flow rate before centralizing. This is not what happened. The results obtained had only an increase in time before centralization.

For the 60 cm tube, the measurements showed that the tube whit smooth surface centralizes almost immediately, but the tube containing rough surface needed 6 seconds before centralization. The vortex core in the 80 cm tube used 25 seconds before centralization with smooth walls, but the one roughened by sandpaper needed 50 seconds.

The interesting part here is that the flow rate needed for centralization are more or less the same for both cases of smooth and rough wall surface. This can indicate that the direct roughening of the walls was not to good and the roughness was too small to affect the EoV.

Configuration [cm]	Flow rate [m^3/h]	Surface	Centralization time [s]
60	65	smooth	1
	65	rough	6
80	60	smooth	25
	60	rough	50

Table 5.10: The difference in wall roughness versus time, from measurement of 60 cm and 80 cm separator tube treated with sandpaper.

5.3.2 Walls Coated with Metal Particles.

For this reason, the walls were coated with metal particles with a mean roughness height of 0.18 - 0.2 mm. The experiments were performed in the same way as the previous ones. Some disadvantage by the use of coating was that the metal powder clogged the pressure tappings along the tube and it was not possible to get pressure measurements from the flowmeter.

Configuration [cm]	Flow rate [m^3/h]	Comments
60	50	NC
	126	NC
	160	NC
	195.4	NC
	229.8	NC
	277.1	C
	341.8	C

Table 5.11: Measurement of the flow rate in a 60 cm tube coated with metal particles.

From the measurements in Table 5.11, the results shows that the vortex core centralizes for a value in the range between 230 m^3/h and 277 m^3/h. For the lower values, it remained attached to the wall.

Another problem with coating of particles was for high flow rates, the precessing vortex core torn the metal particles from the wall, and went along with the clean airstream from the feed. It is possible that the vortex could become affected by it.

Comparisons of the point where the vortex bends off to the wall and where it centralizes are given in a plot in Figure 5.12. These measurements indicates that the roughness surface of 0.1 mm when it is treated with sandpaper has very little influence of the EoV. Measurements with wall roughness of 0.2 mm containing metal particles showed a huge difference in flow rate required for centralization.

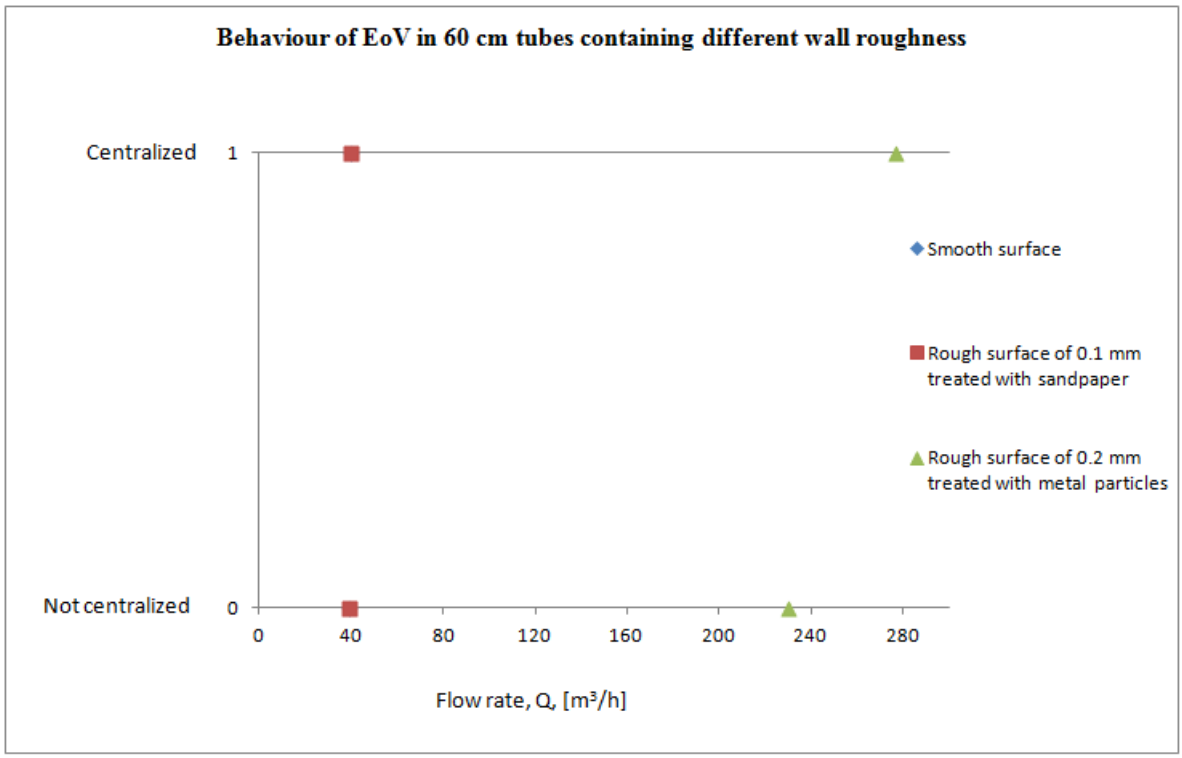

Figure 5.12: A presentation of the EoV where the vortex centralizes in 3 tubes of 60 cm, containing different inner wall roughness.

Measurements of the 80 cm separator body, centralization did not take place at any tested flow rates up to 500 m^3/h. Each experiments were individually run for more than 4 minutes.

The plot in Figure 5.13 shows an overview over the results from the measurements on the 80 cm separator tube. The flow rate is plotted versus centralization. Results from these measurements have the same indications as for the tubes of 60 cm which are treated with sandpaper. The wall surface of 0.2 mm treated with metal particles on the other hand influences the EoV dramatically since the vortex never got centralized for any tested flow rates.

5.3.3 Computational Results

Numerical simulation of the vortex flow in swirl tube containing swirl vanes is carried out to investigate the effect of surface roughness. The results are compared to the effect of smooth surface on the flow field.

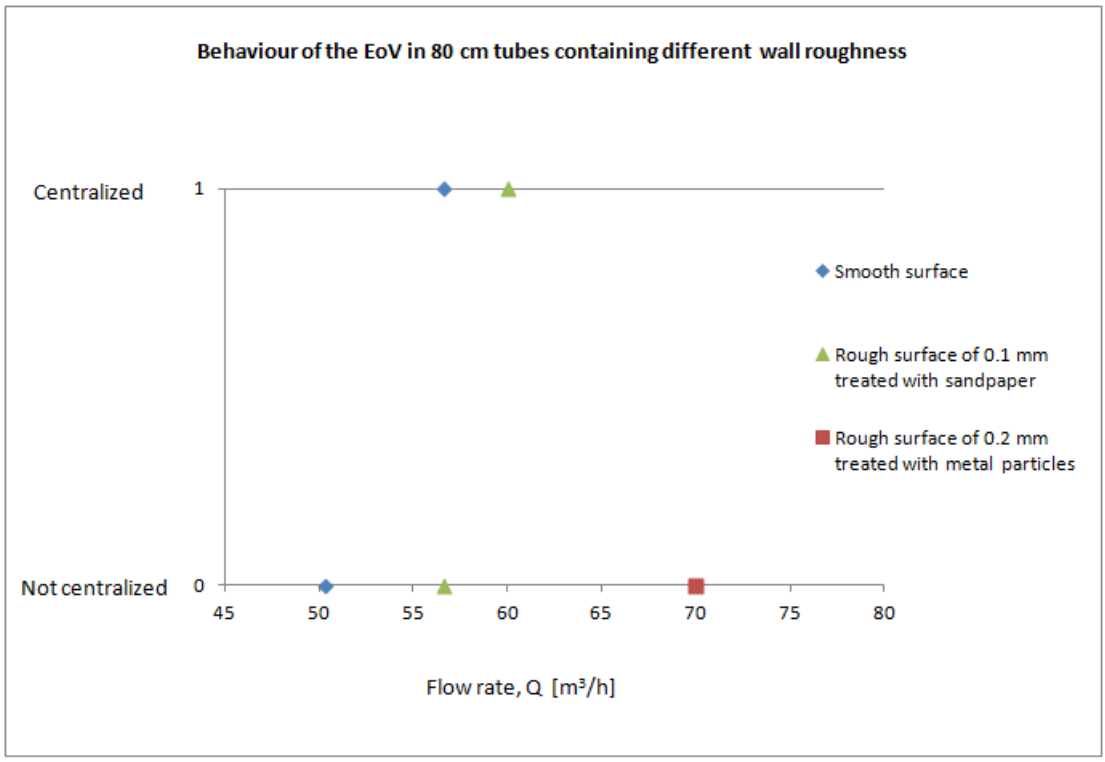

Figure 5.13: A presentation of the EoV where the vortex centralizes in 3 tubes of 80 cm, containing different inner wall roughness.

CFD simulations were performed in three series containing different surface roughness. One containing smooth surface, and two series which had different size of roughness height. The friction factor f was varied. In the program, this was done by changing the parameter E, which is the wall function coefficient. For smooth walls, the parameter was 9 which is standard for the "universal velocity profile" as mentioned in chapter 2.7.3. The values of 2 and 1.2 were used for the two cases involving rough surface. Their roughness height is around 0.1 mm when the parameter E=2, and around 0.2 mm when E=1.2. The accurate values had to be calculated for each running experiments since the roughness depends on the inlet velocity and the shear stress. The inlet velocity were varied between 20 m/s and 60 m/s, which corresponds to 100 m^3/h and 300 m^3/h. The computational results is given in Table 5.12.

Figure 5.14 gives a picture off how the vortex looks in simulations for a centralized case, and in the case where the vortex is attaching itself to the wall and precess around at the same place.

Figure 5.15 shows a series of pictures from a simulation with flow rate of 200 m^3/h. The figure shows how the pressure profiles change when the vortex moves downward and reaches the bottom of the separator tube. The pressure is at its highest at the position before the swirl vanes. As the vortex moves down, the pressure reduces slightly, and it is at its lowest after it has reversed itself, right before it reaches the vortex finder on its way up and out.

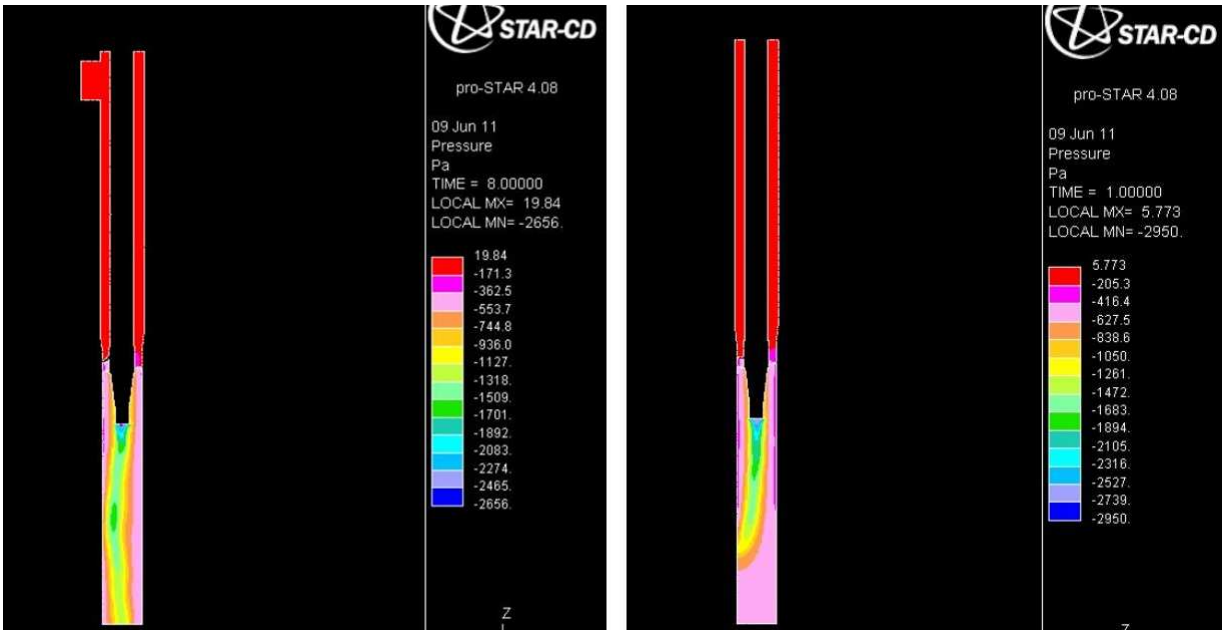

Figure 5.14: CFD simulation with flow rate of 200 m^3/h. Left side shows a centralized vortex. The right side gives a picture of how a precessing vortex looks.

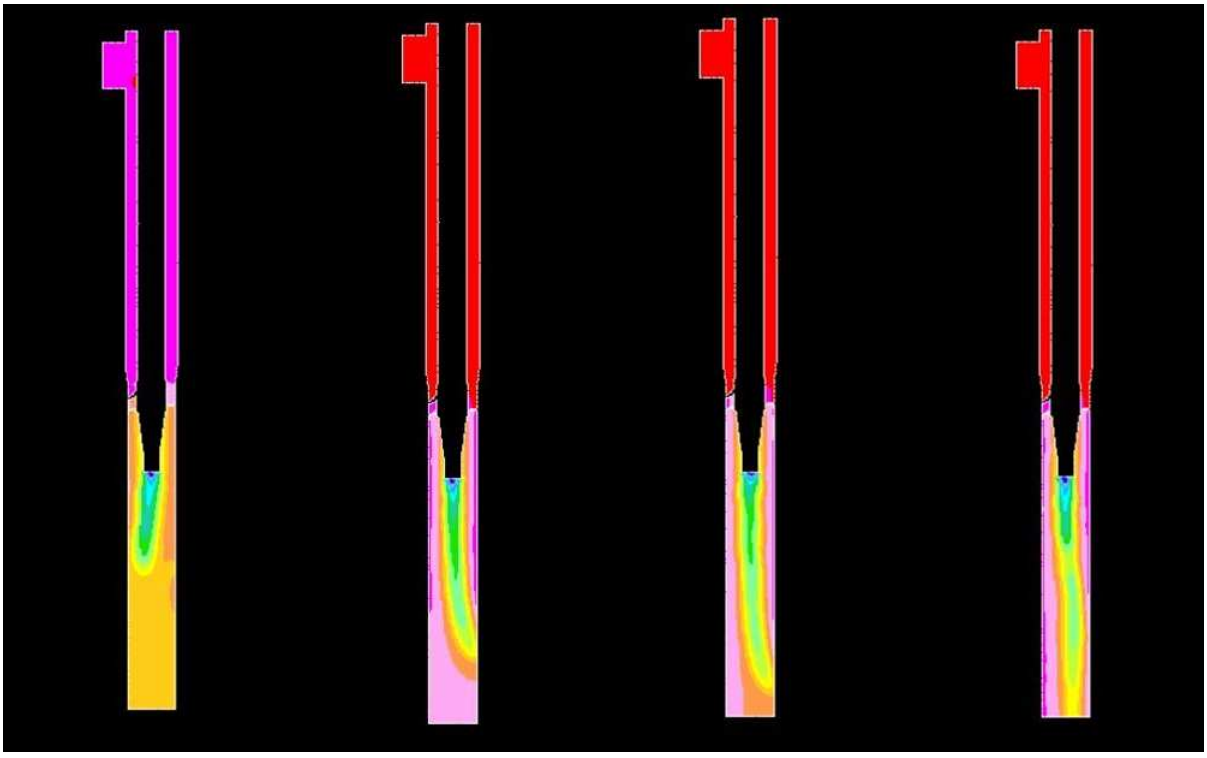

Figure 5.15: CFD simulation with flow rate of 200 m^3/h.

The vortex bended off to the wall before it moved down and centralized for all running measurements in CFD.

E	9	2	1.2
Flow rate [m^3/h]			
100	NC	NC	NC
150	NC	NC	NC
175	C	NC	NC
200	C	NC	NC
225	C	C	NC
250	C	C	C

Table 5.12: CFD results for the 60 cm swirl tube.

Pisarev et al. [33], which is in written moment in print, have performed CFD simulations of an 80 cm separator tube which matches the one in this thesis. The trend in his results were the same as in this thesis. The tube with smooth surface, E=9, centralized for lower value of flow rates, than the ones containing rough surfaces of E=2 and E=1.2. His results showed that the length of separator tube was an important factor for the centralization of the vortex. The 80 cm tube compared to the tube of 60 cm needed higher flow rates before centralization independently of the wall surfaces. This was also detected in chapter 5.1 in this thesis as well.

5.3.4 Comparison of Experimental and Numerical Results

Based on the results from CFD simulations for the EoV in swirl tubes, different values of the flow rate needed for centralization with different wall roughness are presented. The trends in CFD simulations are comparable with experimental data, but not the exact flow rates.

In CFD, the flow rate needed for centralization is 175 m^3/h for a 60 cm separator tube containing smooth wall surface. In experiments for a 60 cm tube with smooth wall surface, the flow rate centralized when it reached 40 m^3/h. This is a pretty huge difference in values of flow rates. The choice of using RSM as the turbulence model rather than LES can be the reason of the qualitative difference in centralization time.

As can be seen from both the numerical and experimental results, the roughness factor had a great impact on the flow rate needed to have the vortex centralized. In experiments, when the roughness height was around 0.2 mm, the vortex became centralized for a flow rate around 250 m^3/h. In numerical results, the exact same flow rate was needed before centralization for the same roughness height as well. These are great results, since they matches each other.

For a roughness height of 0.1 mm, the experimental results showed that the only difference on the tubes were the difference of time before centralization. The flow rate needed for centralization was the same for both.

The numerical simulations could maybe be more accurate comparing to the experimental if the cell size had been smaller. In present simulations, the number of cells were 172 000. Each experiments where run for 20 seconds of real time, and it took about 6 days of simulations. If the number of cells had been increased, the simulation time would have been too long, which again would not be possible to complete.

5.4 Sources of Error

In the present work, several sources of error could have occurred during the experiments. For the experimental measurements on the test rig, the main source of error could be the waiting time between each running measurement. If the centrifugal pump was shut down for too short period of time, some residual flow would still be left in the tube. The new measurement could be affected by that in a way that it centralizes for lower values of flow rate than it would normally do.

Another problem could also be the small amount of dust inserted at the bottom of the tube to make the vortex visible at the bottom. Even though the amount was very small, it could still affect the vortex core at the bottom of the tube before the vortex reversed itself and went out through the vortex finder.

The huge amount of dust inserted from the top of the separator to make the vortex visible through the separator body affects the vortex core, and it needs higher values of flow rate before centralization. This has to do with the density of the gas which changes when another substance influences it. These results are used to visualize the vortex and not used to conclude anything.

By the use of pressure measurements, the pressure tappings should have been closer to each other to be able to achieve a more accurate position of were the vortex bends off to the wall.

The main problem from the measurements containing rough wall surface were, as mentioned in chapter 5.3.2, the way the tubes containing metal particles were treated. When the measurement had been ongoing for a while, the particles were torn up by the downward directed vortex core and a large amount of particles gathered on the bottom of the separator tube. This could maybe affect the behaviour of the vortex.

Chapter 6

Conclusions

The end of the vortex has been observed by using two different experimental methods and by numerical simulations. The first method was visualizing the end of the vortex with a huge amount of dust inserted at the top of the swirl tube. The other experimental method was by use of high resolution pressure transducers. For numerical methods, CFD simulations was performed.

By the use of too much dust, the axial position of the vortex changed. An increase of dust into the cyclone destabilized the vortex in a way that its position moved upwards. If the incoming gas flow was increased, the vortex core would cause the end to move down, and the vortex core would be stabilized.

The results from the new swirl tube with no connections on the separator body showed that the new configuration centralizes the vortex for lower values than it did for tubes with more than one connections. The extensions between the connections on the tube affects the vortex in a way that it needs a higher flow rate to centralize at the bottom of the tube.

The position of EoV at the wall at several flow rates was measured with high resolution pressure transducers. Immediately after start up, the pressure transducers located a drop in pressure when the vortex end attached itself to the wall. The position of attachment was somewhere between 29 cm and 31 cm below the swirl vanes. This was the case for all the experiments.

Experimental and numerical results gave a qualitative agreement. The difference between the two set of results can be due to the RSM turbulence model used in CFD simulation.

A relationship between the experimental and numerical investigation was obtained when it came to the effect of wall roughness on EoV. The influence on EoV increased with an increase in wall roughness. The flow rate needed higher values before centralization for both the experimental measurements and the numerical simulations.

Chapter 7

Further Research

The next step of this project could be to investigate how the EoV would behave with another shape of geometry. There are many opportunities to change the geometry in swirl tubes, for instance the different size and shape of the vortex finder could be looked at.

An interesting thing could be to insert a coloured gas, with approximately same density as air, instead of particles to trace the vortex as it moves inside the separator tube. It could be easier to visualize the vortex this way.

It would also be interesting to see the behaviour of the EoV by using a dust hopper to collect the captured particles in the swirl tube. One could observe if an underflow would appear from the hopper section, and see how that would affect the vortex.

More experiments on the wall roughness should be performed. For these experiments, tubes containing various lengths and other wall roughnesses should be used.

One could try to come up with a new model for the natural vortex length using CFD simulations. Different models containing different geometry parameters, shapes and sizes could be built inside the program. One could see if there are a significant differences for the cylinder-on-cone shaped cyclone and cyclones shaped like swirl tubes with cylindrical shapes.

Appendix A

Venturi Flowmeter

If nothing else is listed, Bentley [5] is used as reference for this chapter.

A venturi flowmeter is one type of differential pressure flowmeters, which are the most common type of industrial flowmeters for clean liquids and gases. The principle with this type of flowmeter is that it has a constriction placed in the pipe and the differential pressure developed across the constriction is measured. The constriction causes a reduction in the cross-sectional area of the fluid. An illustration of a venturi flowmeter is shown in Figure A.1.

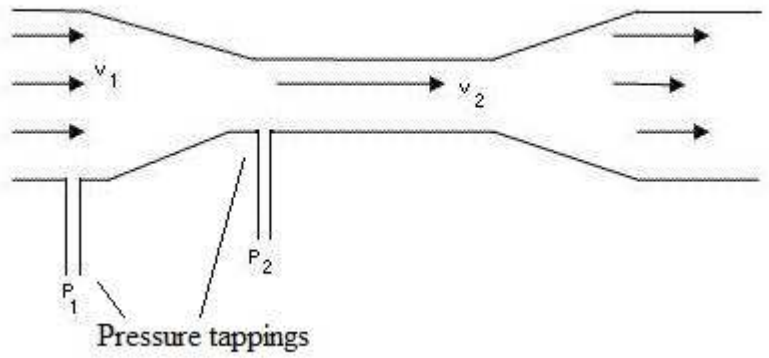

Figure A.1: An illustration of a venturi flowmeter. The figure shows that the velocity is faster in the neck section, which in turn gives a lower pressure.

To be able to come up with a theoretical calculation for the flow rate, some assumptions had to be made to calculate the pressure difference. Since the difference in density for air is so small over the cross sectional area, it can be assumed to be incompressible. We assume that we have a frictionless flow, which means we have no energy loss due to friction and that there are no change in temperature between the fluids and its surroundings.

From chapter 2.3, we recall the Equation (2.4) difference from static and dynamic pressure in Bernoulli's trinomial equation. We assume that we have conservation of total energy.

$$E_1 = \frac{P_1}{\rho} + \frac{1}{2}v_1^2 + gz_1 = E_1 = \frac{P_1}{\rho} + \frac{1}{2}v_1^2 + gz_1 \tag{A.1}$$

Where E is the conservation of total energy and includes pressure energy, kinetic energy and the potential energy.

We have a horizontal pipe which gives $z_1 = z_2$. The Equation (A.1) reduces to:

$$\frac{v_2^2 - v_1^2}{2} = \frac{P_1 - P_2}{\rho} \tag{A.2}$$

Since the flow rate needs to remain constant the whole time even though the cross sectional area, A, decreases we need conservation of volume flow rate:

$$Q_1 = Q_2 = Q \tag{A.3}$$

where

$$Q = A_1 v_1 = A_2 v_2 \tag{A.4}$$

Equation (2.4) and (A.4) combind gives the equation:

$$Q = \frac{A_2}{\sqrt{1 - \left(\frac{A_2}{A_1}\right)^2}} \sqrt{\frac{2\left(P_1 - P_2\right)}{\rho}} \cdot 3600 \tag{A.5}$$

This is the theoretical equation for incompressible flow through a differential pressure flowmeter, and the flow rate is given in m^3/h. This equation is not suitable to use for flowmeters because the flow rate will be smaller, and the geometrical conditions are the one causing it. Because of this, the theoretical equation is being modified by introducing a correction factor termed the coefficient of discharge C_d:

$$Q = \frac{C_d A_2}{\sqrt{1 - \left(\frac{A_2}{A_1}\right)^2}} \sqrt{\frac{2\left(P_1 - P_2\right)}{\rho}} \cdot 3600 \tag{A.6}$$

where

$$A = \frac{\pi D^2}{4} \tag{A.7}$$

The venturi flowmeter used in the experiments had a reported value C_d of 0,9.

Appendix B

Tables

In this Appendix, tables containing all measurements performed on the experimental test rig at different lengths of separator tubes are given. The flow rate was investigated to figure out for which value it centralized or bended of to the wall.

Configuration [cm]	**Flow rate [m^3/h]**	**Comments**
60	9.2	NC
	11.5	NC
	39.4	NC
	41.5	C in 30 seconds
	44.3	C
	72.1	C

Table B.1: Measurement of the flow rate in a 60 cm tube with smooth walls. NC means not centralized, and C stands for centralized.

Configuration [cm]	Flow rate [m^3/h]	Comments
60	22.4	NC
	24	NC
	26.5	NC
	28.5	NC
	29.9	NC
	30	NC
	32	NC
	34.1	NC
	37.2	C in 3 seconds. Too short waiting time before restarting the pump.
	37.5	NC
	37.9	NC
	38.3	NC
	38.5	NC
	39.2	NC
	39.4	NC
	39.7	C in 35 seconds
	39.8	C in 23 seconds
	40.2	C in 20 seconds
	40.9	C in 20 seconds
	41.5	C in 19 seconds
	66.2	C in 1.5 seconds

Table B.2: Measurement of the flow rate in a 60 cm tube with smooth walls.

Configuration [cm]	Flow rate [m^3/h]	Comments
80	58.2	NC
	67	C in 17 seconds
	78	C
	156.6	C in 3 seconds

Table B.3: Measurement of the flow rate in a 80 cm tube with smooth walls.

Configuration [cm]	Flow rate [m^3/h]	Comments
80	30.0	NC
	41.3	NC
	50.3	NC
	56.6	C in 51.6 seconds
	67.3	C in 15.5 seconds
	78.0	C immediately

Table B.4: Measurement of the flow rate in a 80 cm tube with smooth walls.

Configuration [cm]	Flow rate [m^3/h]	Comments
100	57.9	NC
	70.5	NC
	85.2	NC
	90.2	C in 45 seconds
	111.5	C in 12 seconds

Table B.5: Measurement of the flow rate in a 100 cm tube with smooth walls.

Appendix C

Standard Deviation of the Pump

Configuration [cm]	**Flow rate [m^3/h]**
60	26.5
	25.2
	26.4
	22.4
	28.4

Table C.1: Measurement of the flow rate in a 60 cm tube at low flow rates.

The equation for the variance is:

$$s^2 = \frac{\sum_{i=1}^{n} (x_i - \overline{x})^2}{n-1} \tag{C.1}$$

and the standard deviation:

$$s = \sqrt{\frac{\sum_{i=1}^{n} (x_i - \overline{x})^2}{n-1}} \tag{C.2}$$

The uncertainty of the standard deviation has to be calculated to find out how reliable it is.

$$s_s = \frac{s}{\sqrt{2\,(n-1)}} \tag{C.3}$$

Appendix D

Measurements with Pressure Transducers

D.1 80 cm swirl tube

For the 80 cm swirl tube the flow rate was measured at two different values of flow rate and compared the same way as in chapter 5.2

D.1.1 The flow rate at 67 m^3/h

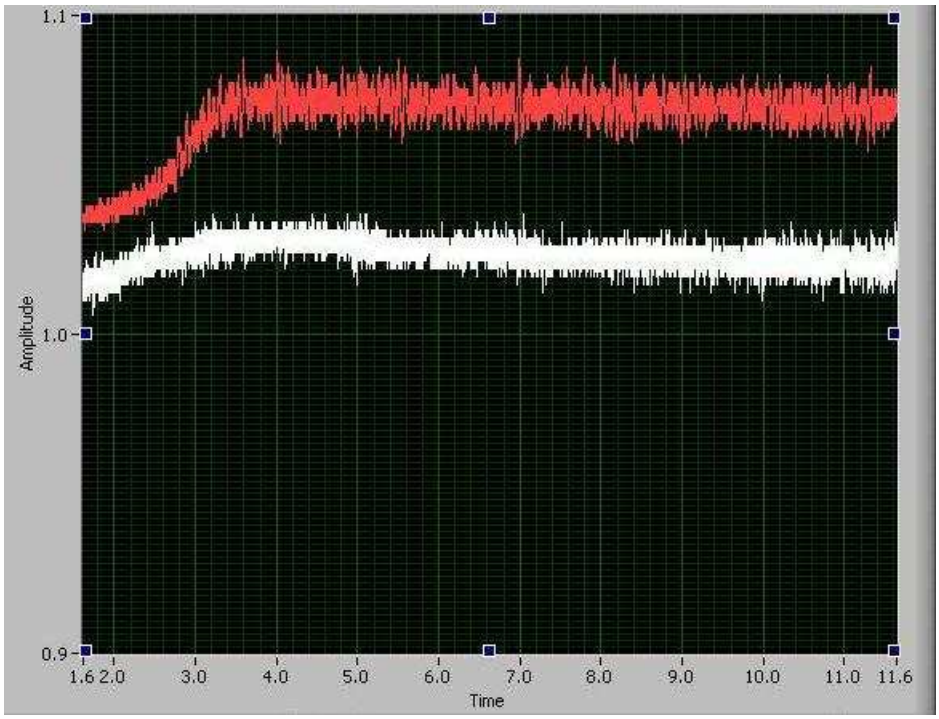

Figure D.1: Output from LabView. Q = 67 m^3/h. Pressure measured at a point 28 cm from the swirl vanes in a 80 cm tube.

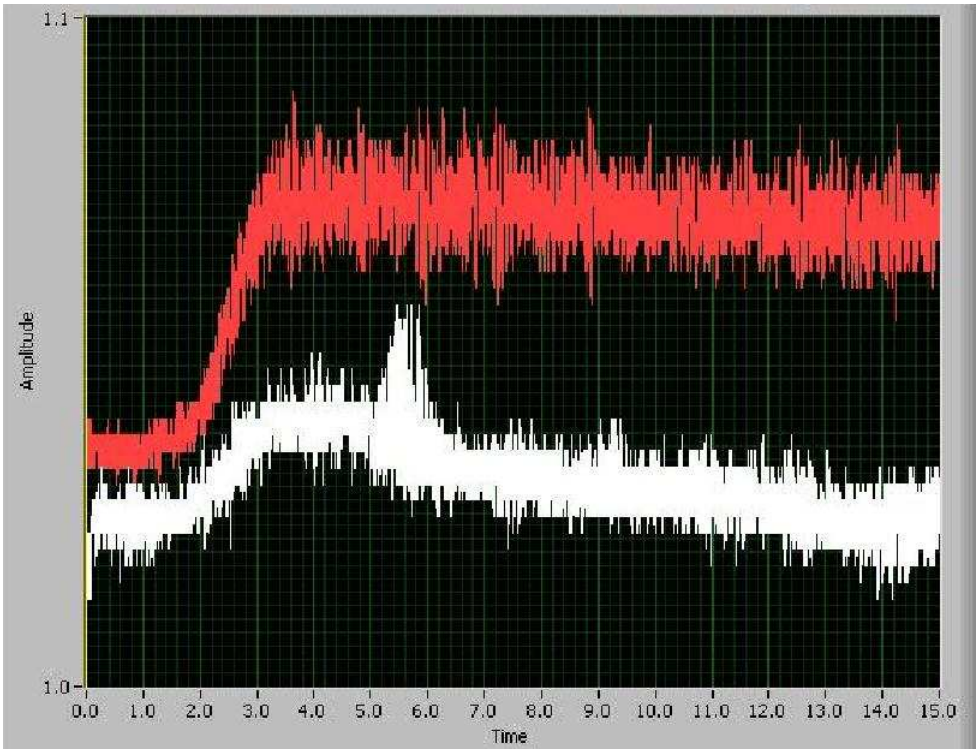

Figure D.2: Output from LabView. Q = 67 m^3/h. Pressure measured at a point 34 cm from the swirl vanes in a 80 cm tube.

In Figure D.1 and D.2, the pressure transducers measured the pressure at a point 28 cm and 34 cm from the swirl vanes. At the point 28 cm from the swirl vanes the picture shows no difference in pressure, but in the figure measured 34 cm from the swirl vanes it gives a trough is present 3 seconds after start up of the pump.

D.1.2 The flow rate at 156.6 m^3/h

From Figures D.3 and D.4 it can be seen that the bending of the vortex is between 28 cm and 34 cm down from the vortex. In Figure D.3 there are no significant difference in pressure after start up, but in Figure D.4 a trough is present 2,2 seconds after start up of the pump.

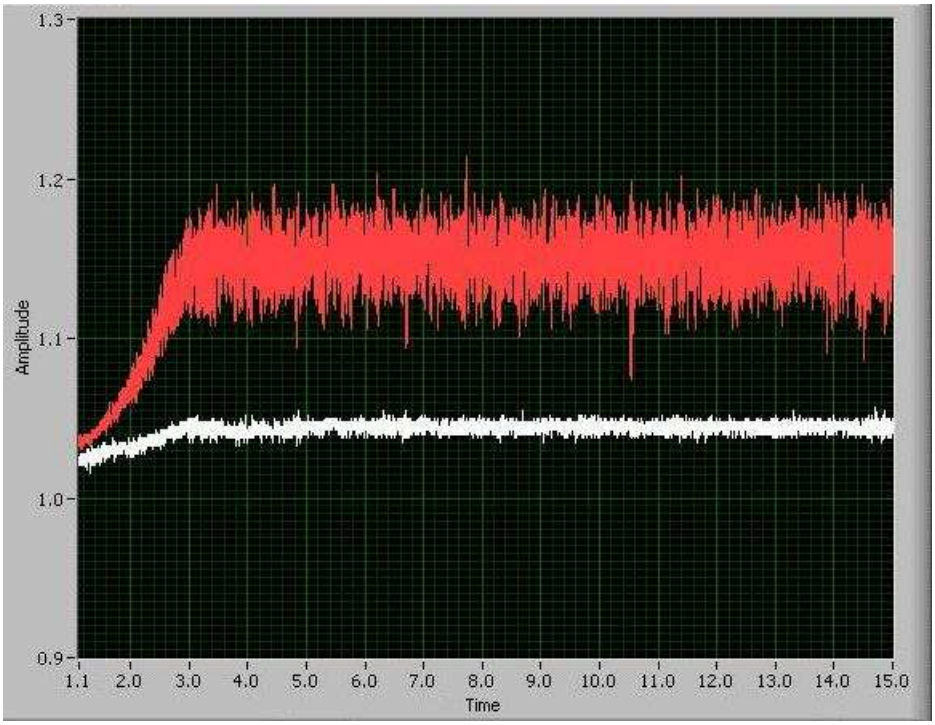

Figure D.3: Output from LabView. Q = 156.6 m^3/h. Pressure measured at a point 28 cm from the swirl vanes in a 80 cm tube.

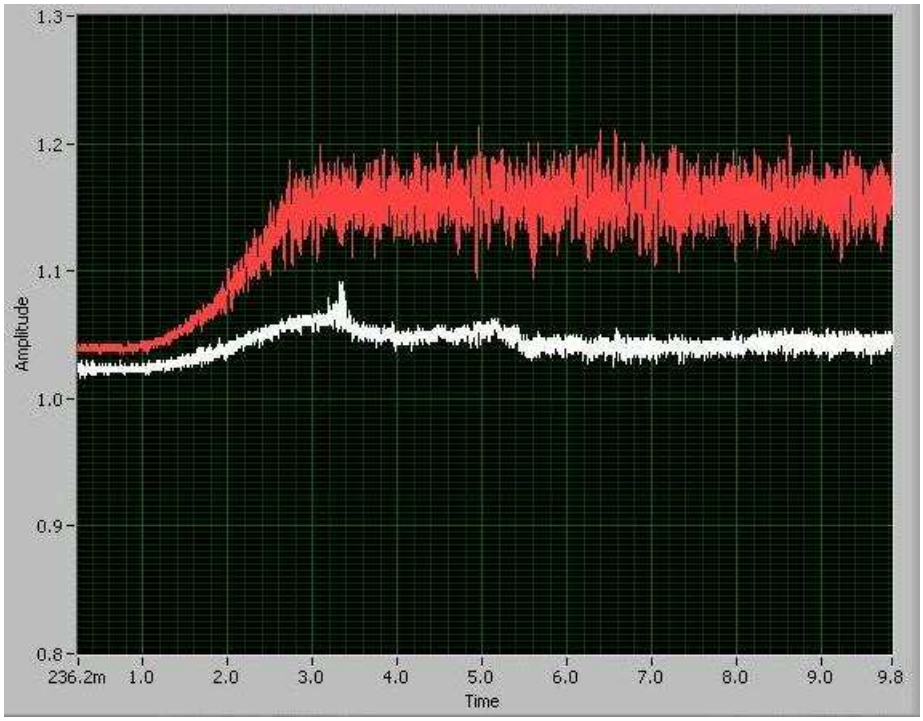

Figure D.4: Output from LabView. Q = 156.6 m^3/h. Pressure measured at a point 34 cm from the swirl vanes in a 80 cm tube.

D.2 100 cm swirl tube

For a 100 cm swirl tube, the flow rate was only measured for one value.

D.2.1 The flow rate at 111.1 m^3/h

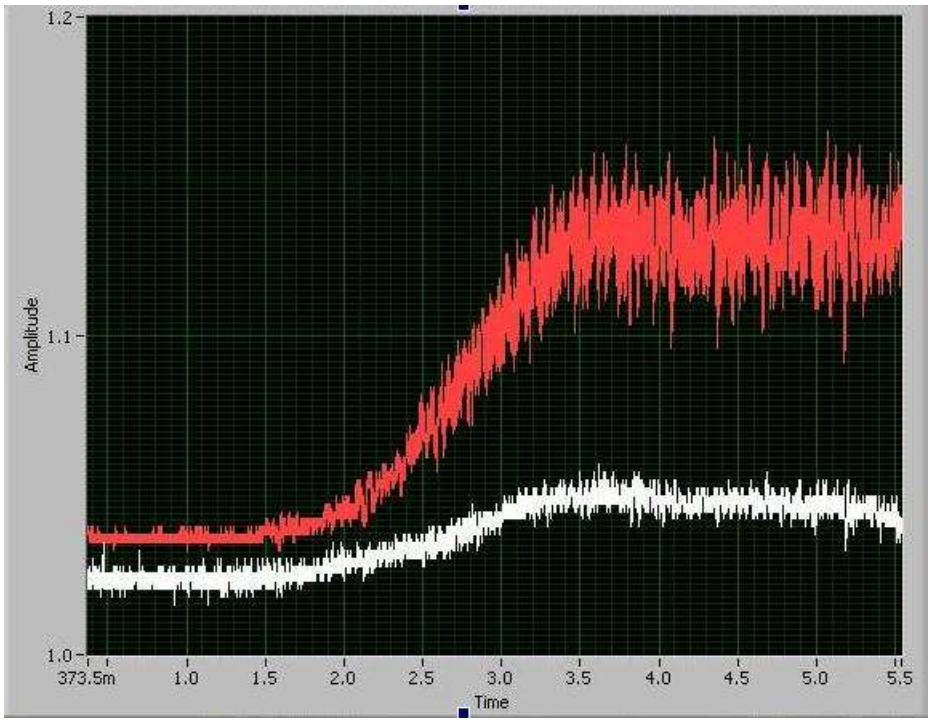

Figure D.5: Output from LabView. Q = 111.1 m^3/h. Pressure measured at a point 28 cm from the swirl vanes in a 100 cm tube.

As can be seen from Figure D.5 and D.6 the vortex bends off to the wall somewhere between 28 cm and 31 cm down from the swirl vanes.

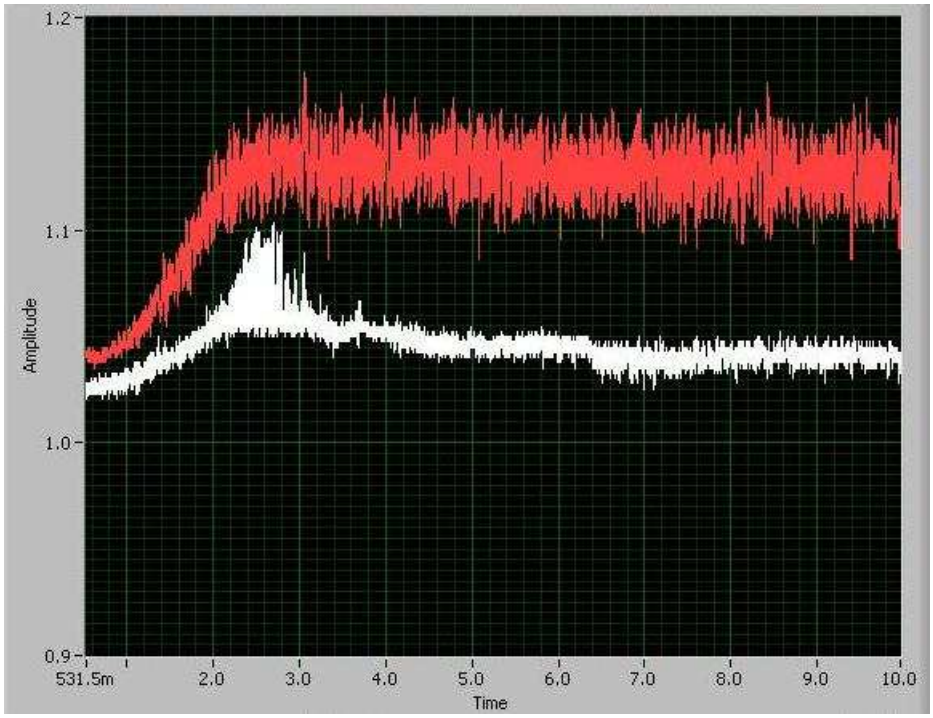

Figure D.6: Output from LabView. Q = 111.1 m^3/h. Pressure measured at a point 31 cm from the swirl vanes in a 100 cm tube.

Bibliography

[1] Alexander, R. M. Fundamentals of cyclone design and operation. *Proceedings of the Australian Institute of minerals and Metals 152/153*, 202-228 (1949). (document), 2.5.1, 2.6.1, 3.1.1

[2] Anderson, J. D. *Computational fluid dynamics: the basics with applications.* McGraw-Hill, New York, c1995. 2.7.1

[3] Azadi, M., Azadi, M., and Mohebbi, A. A cfd study of the effect of cyclone size on its performance parameters. *Journal of Hazardous Materials 182*, 1-3 (10 2010), 835–841. 2.7

[4] Batchelor, G. K. *An introduction to fluid dynamics.* Cambridge University Press, Cambridge, 1967. 2.5

[5] Bentley, J. P. *Principles of measurement systems.* No. 4th ed. Pearson/Prentice Hall, Harlow, 2005. A

[6] Bernardo, S., Mori, M., Peres, A. P., and DionÌsio, R. P. 3-d computational fluid dynamics for gas and gas-particle flows in a cyclone with different inlet section angles. *Powder Technology 162*, 3 (3 2006), 190–200. 1.2, 2.7.1, 2.7.2, 2.7.2

[7] Bryant, H. S., Silverman, R. W., and Zenz, F. A. How dust in gas affects cyclone pressure-drop. *Hydrocarbon Processing 62*, 87-90 (1983). 2.5.1, 2.6.1

[8] Chen, M. Characteristics of the vortex structure in the outlet of a stairmand cyclone: Regular frequencies and reverse flow. Master's thesis, University of Alberta, Department of Chemical and Material Engineering, Edmonton, Fall 1999. 2.2, 2.2.3, 2.4, 2.4.3, 2.7.1, 2.7.2, 2.7.2

[9] Cooper, C. D., and Alley, F. C. *Air pollution control: a design approach.* No. 2nd ed. Waveland Press, Prospect Heights, Ill., c1994. 1.2.2

[10] Derksen, J. J., and Van den Akker, H. E. A. Simulation of vortex core precession in a reverse-flow cyclone. *AIChE Journal 46*, 7 (2000), 1317–1331. 2.7.2

[11] Ferziger, J. H., and Peri, M. *Computational methods for fluid dynamics.* No. 3rd, rev. ed. Springer, Berlin, c2002. 2.7.2, 2.7.2, 2.7.2

[12] Gao, C., Sun, G., Dong, R., and Fu, S. Characterizing the dynamic property of the vortex tail in a gas cyclone by wall pressure measurements. *Fuel Processing Technology 91*, 8 (8 2010), 921–926. (document), 1.2.1, 2.6.1, 3.1.4

[13] Gaupta, A. K. *Swirl flows*. No. OSTI ID: 5976500. Technomic Publishing Co.,Lancaster, PA, Technomic Publishing Co., 851 New Holland Ave., P.O. Box 3535, Lancaster, PA 17604, 1984. 2.5.1

[14] Giaotti, D. B., and Stel, F. *The Rankine Vortex Model*. PhD thesis, University of Trieste, Physics of the Atmosphere, International Centre for Theoretical Physics, Regional Meteorological Observatory, via Oberdan, 16/A I-33040 Visco (UD), ITALY, October 2006. 2.1

[15] Gil, A., Cortès, C., Romeo, L. M., and Velilla, J. Gas-particle flow inside cyclone diplegs with pneumatic extraction. *Powder Technology 128*, 1 (12 2002), 78–91. 1.2

[16] Gjerde, V. I. The natural vortex length in centrifugal separators. Master's thesis, University of Bergen, Department of Physics and Technology, August 2010. 1.4, 2.5.1, 4.8, 5.1

[17] Hoffmann, A. C., de Jonge, R., Arends, H., and Hanrats, C. Evidence of the 'natural vortex length' and its effect on the separation efficiency of gas cyclones. *Filtration & Separation 32*, 8 (9 1995), 799–804. (document), 2.5.1, 2.5.1, 2.5.1, 2.5.1, 2.5.1, 2.5.1, 2.6.1, 3.1.2

[18] Hoffmann, A. C., and Stein, L. E. *Gas Cyclones and Swirl Tubes: Principles, Design and Operation*. No. Second Edition. Springer-Verlag Berlin Heidelberg, Berlin, Heidelberg, 2008. 1.2, 1.2.1, 1.2.2, 2.1.1, 2.2.1, 2.2.2, 2.2.4, 2.3, 2.4.1, 2.4.2, 2.5, 2.5.1, 2.7.2

[19] Hoffmann, A. C., and Stein, L. E. *Gas cyclones and swirl tubes: principles, design and operation*. Springer, Berlin, c2002. 1.1, 1.2, 1.2.1, 1.2.1, 1.2.2, 2.1, 2.1.1, 2.5.1, 2.6

[20] Hoffmann, A. C. a. The effect of the dust collection system on the flowpattern and separation efficiency of a gas cyclone. *The Canadian Journal of Chemical Engineering 74*, 4 (11 1996), 464–470. 2.5.1

[21] Kaya, F., Karagoz, I., and Avci, A. Effects of surface roughness on the performance of tangential inlet cyclone separators. (document), 1.2, 2.3, 2.5.1, 2.5.1, 3.2.1

[22] Kumar, N. A seminar report on computational fluid dynamics. `http://www.scribd.com/doc/50940791/report`. 2.7, 2.7.2

[23] McCabe, W. L., Harriott, P., and Smith, J. C. *Unit operations of chemical engineering*. No. 7th ed. McGraw-Hill, Boston, c2005. 2.5.1, 2.5.1

[24] Mihelcic, J. R., Zimmerman, J. B., and Auer, M. T. *Environmental engineering: fundamentals, sustainability, design*. Wiley, Hoboken, N.J., 2009. 1.1

[25] Peng, W., Christensen, D., Jacobsson, S., Kvinnesland, E., and Hoffmann, A. C. Studies of the flow in and around gas dedusters and demisters using neutrally buoyant tracer. *Chemical Engineering Journal 158*, 1 (3 2008), 11–18. 2.5.1

[26] Peng, W., Hoffmann, A. C., Boot, P. J. A. J., Udding, A., Dries, H. W. A., Ekker, A., and Kater, J. Flow pattern in reverse-flow centrifugal separators. *Powder Technology 127*, 3 (11 2002), 212–222. 1.2.2, 2.1, 2.4, 2.2.2, 2.2.3, 2.2.4

[27] Peng, W., Hoffmann, A. C., and Dijkstra, H. A. A model for the natural vortex length in centrifugal separators. project description, 2007. 1.1

[28] Peng, W., Hoffmann, A. C., and Dries, H. Separation characteristics of swirl-tube dust separators. *AIChE Journal 50*, 1 (2004), 87–96. 1.2.2, 2.5.1, 2.5.1

[29] Peng, W., Hoffmann, A. C., Dries, H., Regelink, M., and Foo, K. K. Reverse-flow centrifugal separators in parallel: Performance and flow pattern. *AIChE Journal 53*, 3 (2007), 589–597. 2.5.1

[30] Peng, W., Hoffmann, A. C., Dries, H. W. A., Regelink, M. A., and Stein, L. E. Experimental study of the vortex end in centrifugal separators: The nature of the vortex end. *Chemical Engineering Science 60*, 24 (12 2005), 6919–6928. (document), 1.3, 2.1, 2.1.1, 2.5, 2.5.1, 2.5.1, 2.5.1, 2.5.1, 2.5.1, 3.1.3, 4.1.3, 5.2

[31] Pisarev, G. I., Gjerde, V. I., Hoffmann, A. C., Peng, W., Balakin, B. V., and Dijkstra, H. A. Experimental and computational study of the 'end of vortex' phenomenon in reverse-flow centrifugal separators. *AIChE Journal*, DOI 10.1002/aic.12695 (2011), 27. (document), 1.2, 1.4, 2.5, 2.7.2, 3.1.5, 4.1, 4.1.2, 4.3, 4.1.3, 4.4, 4.9, 4.3.1, 5.2, 5.3

[32] Pisarev, G. I., Hoffmann, A. C., Peng, W., and Dijkstra, H. A. Large eddy simulation of the vortex end in reverse-flow centrifugal separators. *Applied Mathematics and Computation 217*, 11 (2 2011), 5016–5022. (document), 1.2, 2.2, 2.5.1, 3.1.6

[33] Pisarev, G. I., Rødland, T., and Hoffmann, A. C. Effect of wall roughness on the 'end of the vortex' phenomenon in cyclone type separators. *In print*, 22. 2.5.1, 2.6.1, 2.7.3, 5.3.3

[34] Postma, R. S., and Hoffmann, A. C. The use of swirl tubes for dedusting. Tech. Rep. 272, World Congress on Particle Technology 3, Brighton;UK, 1998. 1.2.2

[35] Qian, F., Zhang, J., and Zhang, M. Effects of the prolonged vertical tube on the separation performance of a cyclone. *Journal of Hazardous Materials 136*, 3 (8 2006), 822–829. 2.5.1, 4.3.1

[36] Qian, F., and Zhang, M. Study of the natural vortex length of a cyclone with response surface methodology. *Computers & Chemical Engineering 29*, 10 (9 2005), 2155–2162. 2.5.1, 2.5.1, 2.6, 2.6.1, 2.6.1, 4.1.3

[37] Raoufi, A., Shams, M., Farzaneh, M., and Ebrahimi, R. Numerical simulation and optimization of fluid flow in cyclone vortex finder. *Chemical Engineering and Processing: Process Intensification 47*, 1 (1 2008), 128–137. 4.1.3

[38] StarCD-adapco. *Methodology*, star-cd version 4.08 ed., 2008. 2.7.2, 2.7.2, 4.3.1

[39] Wan, G., Sun, G., Xue, X., and Shi, M. Solids concentration simulation of different size particles in a cyclone separator. *Powder Technology 183*, 1 (3 2008), 94–104. 2.7.2

[40] Wang, B., Xu, D. L., Chu, K. W., and Yu, A. B. Numerical study of gas-solid flow in a cyclone separator. *Applied Mathematical Modelling 30*, 11 (11 2006), 1326–1342. 4.3.1

[41] Yazdabadi, P., Griffiths, A., and Syred, N. Characterization of the pvc phenomena in the exhaust of a cyclone dust separator. *Experiments in Fluids 17*, 1 (1994-06-24), 84–95, doi: 10.1007/BF02412807. 2.5.1, 2.5.1

[42] Zhongli, J., Xiaolin, W., and Mingxian, S. Experimental research on the natural turning length in the cyclone. *Filtech Conference: Papers S*, 1-2 (1991). 2.5.1, 2.6.1, 2.6.1, 2.6.1

[43] Zhou, L. X., and Soo, S. L. Gas–solid flow and collection of solids in a cyclone separator. *Powder Technology 63*, 1 (10 1990), 45–53. 2.7.2